Volume 1 | Number 1 | Jan 2013 | Pages 1–100

Energy &
Environmental
Science

www.rsc.org/ees

ROYAL SOCIETY
OF CHEMISTRY

ROYAL SOCIETY
OF CHEMISTRY

www.rsc.org/ees

A general framework for the assessment of solar fuels technologies

Jeffrey A. Herron, Jiyong Kim[1], Aniruddha A. Upadhye, George W. Huber, Christos T. Maravelias*

Department of Chemical and Biological Engineering,

University of Wisconsin – Madison, Madison, WI 53706, USA

*   Corresponding author: Tel.: +1 608 265 9026; Fax: +1 608 262 5494. E-mail: maravelias@wisc.edu

Abstract

The conversion of carbon dioxide and water into fuels in a solar refinery presents a potential solution for reducing greenhouse gas emissions, while providing a sustainable source of fuels and chemicals. Towards realizing such a solar refinery, there are many technological advances that must be met in terms of capturing and sourcing the feedstocks (namely CO_2, H_2O, and solar energy) and in catalytically converting CO_2 and H_2O. In the first part of this paper, we review the state-of-the-art in solar energy collection and conversion to solar utilities (heat, electricity, and as a photon source for photo-chemical reactions), CO_2 capture and separation technology, and non-biological methods for converting CO_2 and H_2O to fuels. The two principal methods for CO_2 conversion include (1) catalytic conversion using solar-derived hydrogen and (2) direct reduction of CO_2 using H_2O and solar energy. Both hydrogen production and direct CO_2 reduction can be performed electro-catalytically, photo-electrochemically, photo-catalytically, and thermochemically. All four of these methods are discussed. In the second part of this paper, we utilize process modeling to assess the energy efficiency and economic feasibility of a generic solar refinery. The analysis demonstrates that the realization of a solar refinery is contingent upon significant technological improvements in all areas described (solar energy capture and conversion, CO_2 capture, and catalytic conversion processes).

---

[1] Current address: Department of Energy and Chemical Engineering, Incheon National University, Incheon 406-772, Korea

1. Introduction

Reducing our greenhouse gas emissions, while improving the global standard of living, is one of the key fundamental challenges of the 21st century. One of the options that has been proposed to reduce greenhouse gas emissions is the conversion of carbon dioxide and water into fuels and chemicals.[1-11] This conversion is challenging because the feedstocks have no energy content, carbon dioxide is usually present as a very dilute molecule (~400 ppm in the air) or present as a mixture of gases, and this process requires substantial amounts of energy that must come from another source. Ideally, the energy for this reaction would come from the sun. Several approaches have been proposed for solar fuel production including solar driven electrochemical, photo-electrochemical and photo-catalytic CO_2 conversion to fuels, CO_2 catalytic conversion using solar-derived hydrogen (e.g. methanol synthesis for CO_2 and H_2[12]), and solar-driven thermochemical processes. A number of ongoing projects are developing this technology including the Joint Center for Artificial Photosynthesis (JCAP, a DOE Energy Innovation Hub), several DOE-sponsored Energy Frontier Research Centers (EFRCs) (e.g. the Argonne-Northwestern Solar Energy Research Center, the Center for Solar Fuel), the Solar Fuels Institute[13], the Research Triangle Solar Fuels Institute[14], Sunshine to Petrol (S2P) at Sandia National Laboratories, the SUNCAT (sustainable energy through catalysis) Center for Interface Science and Catalysis, Liquid Light[15], ETOGAS,[16] and SOLAR-JET.[17]

While the field of solar fuels is in its infancy, we believe that evaluating the technologies at a conceptual process level is crucial to help evaluate the realistic viability of proposed solar fuel technology and identifying the critical research that must be done to make a future technology successful. In this review, we will describe and assess, *from a systems-level perspective*, various technologies involved in the renewable production of chemical fuel using solar energy and CO_2 as the primary carbon source (see Figure 1). In the first half of this review, we describe the important feedstocks for a solar refinery (solar energy, H_2O and CO_2), the state of technologies for capturing CO_2 from different sources, and the methods of converting CO_2 to fuels using solar energy. CO_2 conversion follows two principal routes (1) catalytic conversion using solar-derived hydrogen, and (2) direct CO_2 reduction with H_2O. In the first route, hydrogen can be produced using solar energy through various technologies, including electrolysis, photo-electrochemical water splitting, photo-catalytic water splitting, and thermochemical methods. In the second route, CO_2 is reduced with H_2O using electrocatalytic, photo-electrochemical, photo-catalytic, or thermochemical methods. In the second half of this review, we demonstrate how these various technologies are integrated into a solar refinery and perform a techno-economic analysis, *using methanol as the final product as a case study*, to assess these technologies. Importantly, through our modeling and analysis, we have identified the critical challenges and key targets for improving the overall economic feasibility of the solar to chemical energy process. The objective of this study is to provide an overview of the current technological approaches being used for solar fuel production and to provide a vision as to where future research efforts should be focused. Importantly we will illustrate the fundamental laboratory discoveries that are needed to turn these technologies into commercial projects.
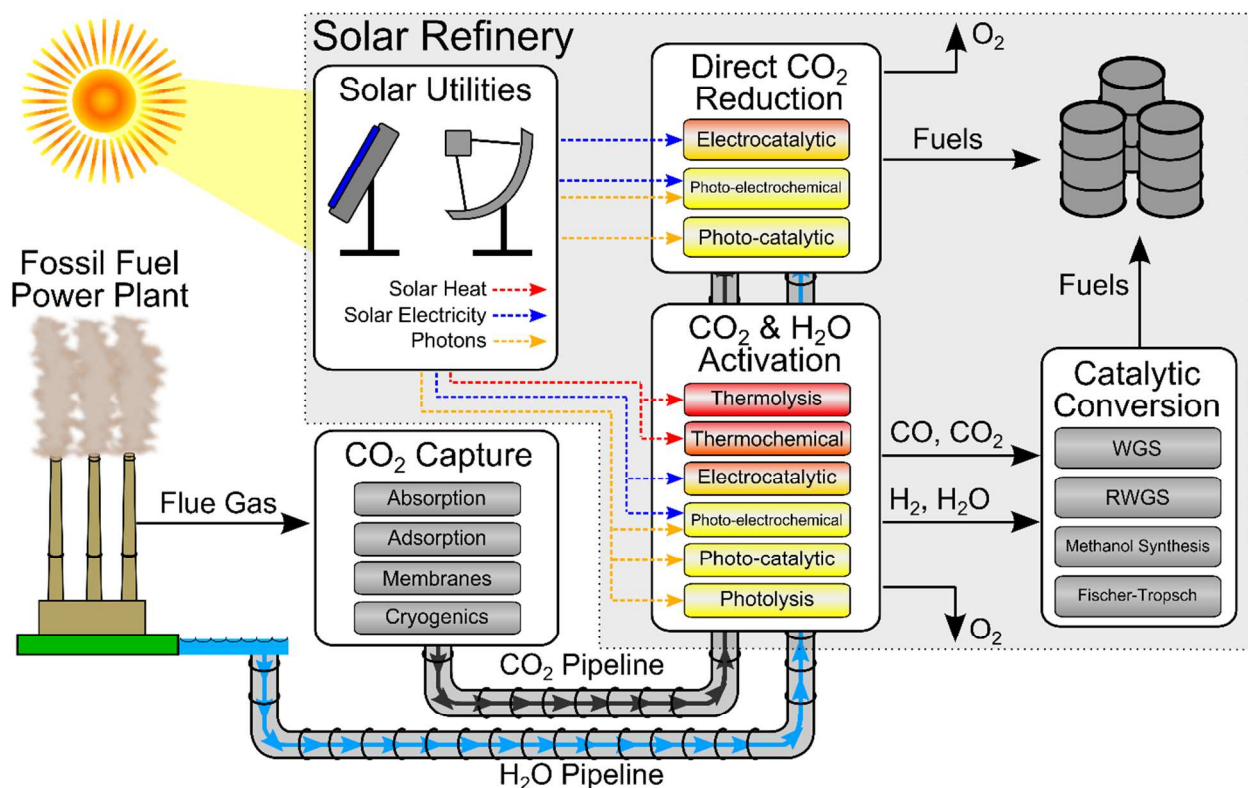
Figure 1. Schematic for solar fuels production. Solar fuel feedstocks (CO_2, H_2O, and solar energy) are captured on-site and/or transported to the solar refinery. Solar energy provides solar utilities in the form of heating, electricity, and photons which are used in the solar refinery to convert CO_2 and H_2O into fuels. CO_2 and H_2O are converted to fuels through two principal routes: (1) direct solar-driven CO_2 reduction by H_2O to fuels or (2) solar activation of CO_2/H_2O to CO/H_2, respectively, and subsequent catalytic conversion to fuels via traditional processing (i.e. methanol synthesis or Fischer-Tropsch). The approximate temperature requirements for the solar-driven conversion processes are color-coded (red = high temperature, yellow = ambient temperature).

2. Solar Fuel Feedstocks

In this section, we will describe the key resources that are required for solar fuels production: solar energy, water, and CO_2. We will describe their availability and the costs to acquire those resources, from both energy and capital perspectives. We will first discuss the solar energy resources, then briefly comment on water resources, and finally describe CO_2 resources (including CO_2 capture and separation technologies).

2.1. Solar Energy Resources

The solar radiation spectrum spans a wide range of wavelengths, and resembles black body radiation at 5777 K as seen in **Error! Reference source not found.**.[18, 19] The energy in solar radiation is proportional to the frequency (*v*) of the light as given by Planck's relation ($E = hv$). More than 25% of the extraterrestrial radiation is absorbed by greenhouse gases such as O_3, CO_2 and H_2O.[20] Of the solar radiation reaching Earth's surface, about 52% of the energy is in the infrared region (>700 nm), 43% is visible-light radiation (400-700 nm) and about 5% is in the

ultraviolet range (<400 nm). The amount of radiation incident on the earth's surface depends upon many factors such as (a) location (latitude), (b) time of the day, (c) inclination of the surface, (d) declination, (e) weather, etc.[19] The resulting intermittent nature of solar radiation is one of the major challenges in designing solar fuels technology. Thus, storing solar energy is critical for continuous processing during these fluctuations. The monthly averaged daily radiation numbers can be calculated using correlations available in the literature.[19, 21] Furthermore, the National Renewable Energy Laboratory (NREL) has databanks and models available which can be used to estimate the solar radiation.[22]
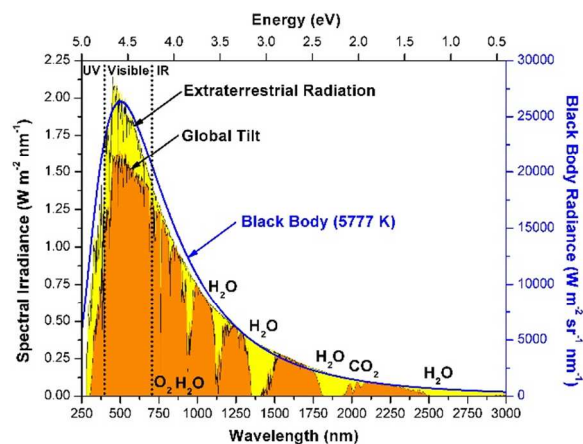

Figure 2. Spectral distribution of solar radiation (i) Extraterrestrial radiation outside earth's atmosphere, (ii) Global total radiation incident on the 37° inclined surface and (iii) black body radiation at 5777 K. Absorption bands for O_2, H_2O, and CO_2 are indicated. (Data adapted from ref[18])

Error! Reference source not found. shows the localization of solar resources throughout the world.[23] The amount of solar energy intercepted by the earth in 1 hour is more than the annual world energy consumption,[3, 24] though it is not uniformly distributed. As seen from the **Error! Reference source not found.**, solar energy resources are abundant in most parts of Africa, the Middle East, Australia, South America, the Indian subcontinent, and Central America. These areas receive more than 6 kWh m^{-2} of solar radiation per day. Northern parts of America, Europe and Asia receive relatively lower solar radiation in comparison. Furthermore, the fluctuations in solar energy availability over time are minimized near equatorial regions, hence these represent promising locations for solar fuels refineries. Though, one must also consider the availability of raw materials such as water and CO_2.
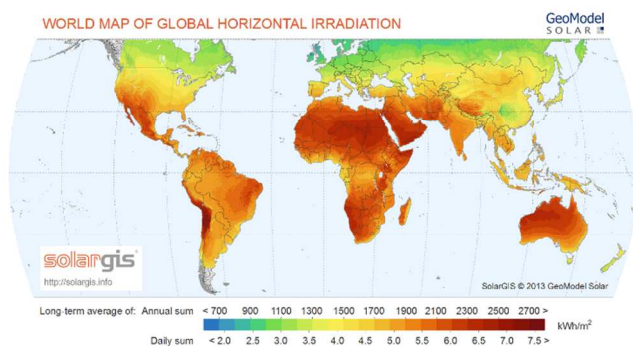
Figure 3. World map of global horizontal solar radiation (figure is reprinted with permission, SolarGIS © 2014 GeoModel Solar[23])

2.1.1. Solar energy collectors: Solar energy is often concentrated prior to its use in industrial processes. In this section, we discuss several different types of solar energy collectors.

With flat surface collectors, the incident light is directly utilized without concentrating. Therefore, the intensity of the solar radiation is limited to a maximum of 1000 W m^{-2} (i.e. the solar energy intensity reaching the earth's surface). Flat surface collectors are often used for domestic solar heating and photovoltaic (PV) applications because of their low cost and ease of installation.[25, 26]

Solar concentrators increase the solar intensity that reaches the receiving surface. Concentration ratios (ratio of radiation intensity at receiver to intensity at the collector) from 1 to 10^5 can be obtained using these devices.[19] Concentrating the solar intensity helps to reduce the amount of expensive PV or catalyst material required in a given process and also allows for the generation of higher temperatures at the receiver. Unfortunately, for photo-catalytic systems as the solar intensity increases, the rate dependence on the solar intensity diminishes from 1 to 0.[27, 28] Solar concentrators can only utilize direct normal solar radiation, unlike flat plate collectors which can utilize diffuse radiation along with direct normal radiation. Reflectors and luminescent[29] solar collectors are two of the most common concentrated solar collectors. The commercial applicability of these concentrators is limited because of issues with stability and lower collection efficiency.

Different configurations of reflective solar concentrators are possible,[19] with parabolic trough and dish collectors being the most common.[25] Parabolic trough collectors use reflectors that are curved around one axis in a parabolic shape, which concentrates solar radiation on one line. Parabolic dish reflector concentrators use 2-dimensional parabolic dishes to concentrate radiation over a small area. The current cost of concentrating solar collectors ranges between 150-250 USD m^{-2}.[30] Sphinx glass, Saint-Gobain, Guardian industries, and 3M are leading technology providers for concentrating solar collectors.

2.1.2. Solar energy utilities: In the solar refinery, solar energy is a utility which can be employed towards different applications. For one, photons can drive chemical reactions in photo-catalytic, photo-electrochemical and photolysis reactions. Additionally, solar energy can be converted into solar heating and solar electricity utilities to drive thermochemical and electrochemical transformations, respectively. Furthermore, solar utilities could also be used in other parts of the refinery as process heating and process electricity. For example, solar heat can be used for separations, which, as we will show in this paper, are very important energy drivers. In this section, we discuss the conversion of solar energy into solar heat and solar electricity.

Solar heat is the most mature application for solar energy. Apart from industrial solar thermal energy,[31] solar energy is widely used for domestic water heating and air heating.[32] It is a low cost application with high energy conversion efficiency. Concentrated solar collectors can be used in

industrial settings to reach temperatures as high as 2000°C.[33] The solar to heat efficiencies obtained from these systems highly depend upon the operating conditions such as the surface temperature and ambient temperature.[19] Though, annual collection efficiencies of ~45% have been reported.[34] Unfortunately, a major drawback for solar heat systems (including solar heat reactors) is that they are highly sensitive to the intermittency (e.g. weather effects) of solar radiation.[35]

There are two main approaches to produce electricity from solar energy: (i) photovoltaics and (ii) solar thermal power.[36] Photovoltaic devices use semiconductor materials to generate direct current electricity from incident light. In contrast, solar thermal power systems use solar energy as a heat source to drive heat engines, which are connected to electrical power generators.

In photovoltaics, when a photon having energy greater than the material's band gap (the separation between the bottom of the conduction band and the top of the valence band) is incident on the material, an electron-hole pair is generated. The recombination of electron-hole pair is minimized by building a potential barrier through a thin-layer of junction, which is created by doping the semiconductor material with n-type (electron-rich) dopants on one side and p-type (hole-rich) dopants on the other side. Electrical current is produced when the sides are connected through an external circuit. The efficiency of photovoltaic cells depends on several factors such as operating temperature[37, 38], operating load, intensity of the radiation, and materials properties.[19] Recent reviews on photovoltaic cell technology are available in the literature.[39-41]

Figure S1 shows the time-evolution of research-cell efficiencies.[42] Based on the material characteristics, the PV cells can be classified into (i) Crystalline Si cells[43], (ii) Single-Junction GaAs Cells[44], (iii) Multijunction cells[44], (iv) Thin-Film Technologies[45] and (v) Emerging PV technologies. Crystalline Silicon cells utilize pure silicon material which has a band gap of 1.12 eV. The best reported efficiency for such materials is 27.6% (the theoretical efficiency (Shockley-Queisser) limit is 29%[46]), and it is obtained with single crystal materials using concentrated solar radiation.[47] GaAs based materials are characterized by a band gap of 1.424 eV. The highest efficiency achieved with these materials is about 29.1% using concentrated solar radiation, with a theoretical Shockley-Queisser limit of 33.5%.[48] Multijunction cells utilize multiple layers of different semiconductors with varying band gaps to boost the overall efficiency of the cells. The materials are stacked in layers such that the incident radiation contacts the layers in order of decreasing band gap. The highest energy photons are absorbed in the first layer, while the lower energy photons pass through to successive layers where they are absorbed. This maximizes the energy efficiency of the system, and the highest reported efficiency of such a system is 44.4%.[49] We note that the theoretical efficiency limit for a tandem solar cell with an infinite number of cells is 86.8%.[50] Because of the high cost of manufacturing crystalline materials, alternative photovoltaic cells have received considerable attention. These include thin-film cells, dye-sensitized solar cells[51, 52], organic photovoltaic cells[53], inorganic cells[54] and quantum cells[55]. Although the highest cell efficiencies obtained with such systems are lower compared with crystalline materials, these materials are very promising in terms of

commercializing PV electricity. The current estimated levelized cost of electricity using PV is expected to be around 144.3 USD MWh^{-1}.[56]

Solar thermal power, often referred to as concentrated solar power (CSP), is an alternative to PV technology.[57, 58] In these systems, concentrated solar energy is used to drive a heat engine at high temperatures to produce electricity. [59, 60] These systems can achieve 20-25% solar to electricity conversion efficiencies.[61] Because of the need to operate at high temperature, these systems are typically large–scale, which results in higher capital costs. Thus, the estimated levelized cost of electricity from such systems is much higher than from PV, 261.3 USD MWh^{-1}.[56] Although the cost of electricity is higher, one of the advantages of these thermal systems is that the cost to store thermal energy is significantly lower than the cost of electrical energy storage in batteries. Energy storage is critical to overcome issues with solar energy intermittency.[62-64]

2.2. Water Resources

Water presents a second key resource in the solar refinery. Water can be directly converted to hydrogen (and oxygen) through a number of different solar technologies as described in Section 3. Alternatively, water can be directly consumed (without forming hydrogen as an intermediate) during CO_2 reduction to various fuels, as described in Section 4. In general, areas which have high solar resource availability may not have high water availability.

In 2005, the estimated daily water withdrawal in United States was 410 billion gallons per day (~1.5 trillion kg day^{-1}).[65] Of those withdrawals, approximately 49% was used for cooling in thermo-electric power plants, 33% for irrigation/agriculture, 11% for public supply, 4% in industry, 1% in mining, and 1% for domestic use. We note that the term "public supply" refers to water withdrawals that serve at least 25 people, and 86% of the U.S. population receives their water in this way. The majority of this water is returned to the source after use (e.g. once-through cooling of power-plant), though estimating the exact consumption is difficult. Even so, in the United States, an estimated 5.9 billion gallons (22.3 billion kg) of water are consumed daily in thermo-electric power plants.[66]

Due to these large withdrawals, there are areas of the United States which already exceed precipitation rates. These areas include the southwest United States, California, Florida and the high plains.[67] Therefore, water may need to be transported to the solar refinery. Based on simulations, we have calculated a cost for water transportation of 0.007 USD MT^{-1} km^{-1}, assuming 15 MT yr^{-1} water capacity. We note that based on the process modeling in Section 5 that this translates into a very small fraction of the overall process cost, therefore we will not discuss this resource further.

2.3. CO$_2$ Sources, Capture and Separation

CO_2 is available abundantly in the air, with 34 billion tons emitted globally in 2011.[68] However, it is in low concentration, approximately 400 ppm (0.04%), which makes it unsuitable for most conversion processes without employing expensive capture and purification methods. Therefore,

it is beneficial to acquire CO_2 from more concentrated sources. In the United States, approximately 38% of CO_2 emissions are from electric power plants, primarily coal-fired plants, and another 18% are from industry,[69] presenting promising sources for CO_2. Excluding CO_2 capture from the atmosphere, there are three main routes for CO_2 capture from these stationary sources: post-combustion, pre-combustion, and from oxy-combustion. Each of these routes have preferred CO_2 capture methods because of the varying physical properties and chemical composition of the capture source (see Table 1).

Post-combustion capture of CO_2 refers to CO_2 separation from flue gases that were created by combustion in air. The flue gas stream consists of 3-20% CO_2 in nitrogen, oxygen and water vapor with some minor impurities including SO_x, NO_x, and particulate matter.[70] Post-combustion capture is relatively easily retrofitted on existing fossil fuel power plants, and presents the most near-term solution to CO_2 capture. Due to the relatively low concentration of CO_2 in the stream, it is best captured through chemical absorption/adsorption and is industrially captured using absorption in monoethanolamine (MEA).

Pre-combustion capture of CO_2 is performed from synthesis gas (syngas) streams prior to combustion/power production, as in integrated gasification combined cycle (IGCC) power plants.[71-73] In these power plants, the fossil fuel is first gasified to produce syngas, which is converted via water-gas shift (WGS) to remove the CO and increase the quantity of H_2. Carbon dioxide is removed from this stream prior to combustion of the hydrogen gas, the stream consists of 15-40% CO_2 at elevated pressure (15-40 bar).[70] Due to the high partial pressure of CO_2 in these streams, physical absorbents/adsorbents and membranes present promising methods for capture.[74]

In an oxy-combustion process, the fuel is combusted in an atmosphere of O_2/CO_2, rather than air. The resulting effluent consists of 75-80% CO_2 in water vapor, with trace amounts of NO_x and SO_x.[70] Some of the CO_2 must be captured and used as a diluent in the oxygen stream to control the temperature of the furnace. It is typical to separate the CO_2 by lowering the temperature to condense the water vapor.[75] Chemical Looping Combustion (CLC)[76] is an alternative oxy-combustion process where the fuel is combusted upon contacting a solid oxygen carrier (e.g. a metal oxide). The depleted oxygen carrier must be re-oxidized, closing the overall loop. This strategy is advantageous because it avoids the high energy costs required to obtain purified oxygen (as in the oxy-combustion process, which is usually by cryogenic oxygen separation from air).

Once CO_2 is captured, it must be transported to the solar refinery for conversion. The current state of CO_2 pipeline infrastructure was recently reviewed,[77] finding approximately 6500 km of CO_2 pipeline worldwide, with the majority in the United States. (We note that these pipelines are mainly employed for enhanced oil recovery.) The cost for CO_2 transportation has been studied by NETL, suggesting a cost of 3.65 USD MT^{-1} for 100 km transport range.[77, 78]

The state of CO_2 capture technology has recently been reviewed by Aaron[79], Choi[80], D'Alessandro[81], Espinal[68], Jones[82], Mondal[83], MacDowell[84], Spigarelli[70], and Folger.[85] Here, we

summarize the four main CO_2 capture/separation technologies: absorption, adsorption, membrane separation, and cryogenic distillation with an emphasis on CO_2 capture from post-combustion flue gases.

Table 1. Sources of CO_2 for capture: properties, and composition.

	Atmosphere	Post-Combustion	Pre-combustion	Oxy-combustion
Pressure (bar)	1	1	15-40	1
CO_2 Concentration	400 ppm	3-20%	15-40%	75-80%
Major Impurities	N_2, O_2	N_2, O_2, H_2O	H_2, CO	H_2O
Lesser Impurities		NOx, SOx, particulates	NO_x, SO_x, H_2S	NO_x, SO_x

2.3.1. Absorption technology: "Wet-scrubbing" CO_2 capture is an industrially mature technology. In the general process (see Figure 4), the gaseous CO_2 stream (i.e. flue gas) flows up an absorption tower, while a liquid solvent flows down the tower. The CO_2 dissolves into the solvent and the CO_2-rich solvent is pumped into a desorption column (regenerator), where it is regenerated by stripping with steam at elevated temperature at near ambient pressure. The choice of solvent varies depending on the composition and conditions of the gas stream. Though, typical physical solvents include glycol ethers (Selexol) and methanol (Rectisol),[86] while the most common chemical solvent is monoethanolamine (MEA) 20-30 wt% in water. The absorption capacity of physical solvents is proportional to the partial pressure of CO_2, and therefore they are advantageous in concentrated CO_2 streams. In contrast, chemical absorption does not have this limitation, and is therefore useful for more dilute streams. In amine-scrubbing, CO_2 reacts with the amine through a zwitterion mechanism to form a carbamate species:

$$CO_2 + 2R_1R_2NH \leftrightarrow [R_1R_2NCO_2^- + R_1R_2NH_2^+]$$

The energy cost for commercial CO_2 capture via the MEA wet-scrubbing has been reported to be as low as 0.37-0.51 MWh ton_{CO2}^{-1},[87] though the energy costs will vary depending on the capture conditions. The CO_2 loading capacity in MEA is 0.40 kg_{CO2} kg_{MEA}^{-1}.[70] Some of the main disadvantages of this process are the high energy cost for regenerating the solvent, the cost to compress the CO_2 for transport and storage, and specifically for the MEA-process, the low degradation temperature of MEA.

Research in the field has primarily focused on finding improved solvents for the process: optimizing CO_2 capacity, heat of CO_2 absorption and rate of CO_2 absorption. One class of promising chemical solvents are sterically hindered amines (e.g. 2-amino-2-methyl-1-propanol, AMP).[84, 88-91] Ionic liquids are a class of promising physical solvents that are advantageous due to their very low vapor pressure, thermal stability, non-flammability, low heats of adsorption (physisorption), and relative ease of tuning.[92-95]

2.3.2. Solid adsorbents: Adsorption on the surfaces of solids presents another possible method of capturing CO_2.[80, 96] Adsorbants are able to remove CO_2 from streams through a variety of mechanisms, including molecular sieving (size-exclusion), physisorption, and chemisorption. After adsorption, CO_2 is desorbed and the adsorbent regenerated through pressure swing or temperature swing systems. The adsorbents are generally classified as low-temperature

adsorbents, which include physisorbents (Metal-organic framework (MOFs), zeolites, and carbon) and chemisorbents (MOFs, supported amines, and polymers); or high-temperature adsorbents, which include metal oxides and hydrotalcites.
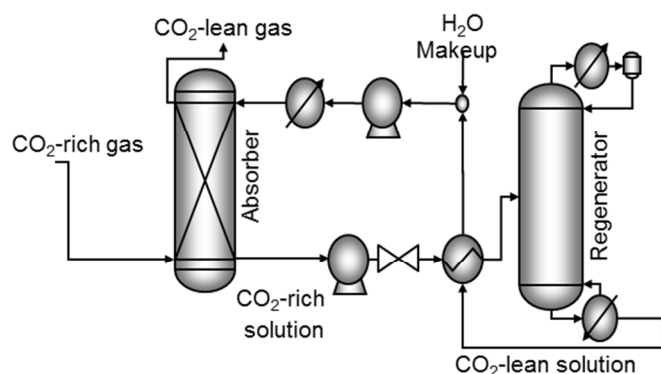

Figure 4. Generic absorption and regeneration process for CO_2 capture. MEA is a typical absorbant used to capture CO_2 from flue gas.

Zeolites are microporous crystalline aluminosilicates composed of SiO_4 and AlO_4 groups. Substitution of an AlO_4 groups with a SiO_4 groups creates a negative charge, which is compensated by a cation (e.g. alkali) in the pores.[97] Metal-organic frameworks are microporous crystalline networks composed of metal centers which are connected by organic ligands.[98-100] MOFs can be produced of a wide variety of structures. As such, they can separate through several different mechanisms, including chemisorption, size-exclusion, and molecular sieving. Supported amines function similarly as solvent amines.[82] There are many methods of supporting the amines: polymeric amines can be physically loaded into the support[101, 102], they can be covalently linked the support[103-105], or by *in situ* polymerization of aminopolymers.[101, 106] Metal oxides (e.g. CaO, MgO) capture and release CO_2 through reversible, carbonate looping. One of the most common materials for carbonate looping is CaO, which forms $CaCO_3$ between 600-650°C in the presence of CO_2 and calcines to regenerate CaO between 800-850°C.[81, 107, 108] Finally, hydrotalcites are a class of anionic clays with the stoichiometry $M^{2+}_{1-x}M^{3+}_x(OH)_2A^{m-}_{x/m} \cdot yH_2O$, where M^{2+} is typically Mg^{2+}, Zn^{2+}, or Ni^{2+}; M^{3+} is typically Al^{3+}, Ga^{3+}, Fe^{3+}, or Mn^{3+}; and A^{m-} includes CO_3^{2-}, Cl^-, SO_4^{2-}, NO_3^-.[109] Adsorption of CO_2 occurs on the basic surface sites. See the supporting information for additional details on these materials.

2.3.3. Membrane separations: Membranes present another method of separating CO_2 from flue gas.[79, 110] Membranes can separate CO_2 through a variety of mechanisms including solution-diffusion transport, molecular sieving, and Knudsen diffusion. Dense polymeric membranes[111], generally, function using the solution-transport mechanism, where CO_2 first dissolves into the membrane and then diffuses across. They have been employed for selective separation of CO_2 versus N_2. The selectivity of these membranes can be improved by improving CO_2 solubility by incorporating species with preferential interactions with CO_2, e.g. amines[112] and ionic liquids.[113] Mixed-matrix membranes have incorporated inorganic nanoparticles to improve membrane properties.[114] With membranes, one of the major problems is that there is an inverse correlation

between selectivity and permeability, therefore the choice of membrane must be optimized for the specific process. Overall, membranes are efficient methods for separating large volumes of gas, if high purity is not required.

2.3.4. Cryogenic separation: Cryogenic distillation is industrially employed to separate air into its constituent components, and presents an option for CO_2 separation from concentrated streams.[75] However, for dilute capture from post-combustion flue gas, the technology is not as developed. Clodic and co-workers have developed a cryogenic CO_2 separation process whereby the flue-gas stream is cooled over several stages to 0°C and then passed through a dehydrator to remove the water.[115, 116] Water must be removed in order to prevent the formation of ice, which may plug the systems. Then, the stream is cooled to -50°C to remove any trace gases and hydrocarbons before the final N_2/CO_2 separation is performed in an evaporator at -110°C, where CO_2 de-sublimates. The CO_2 is recovered as a liquid by heating to -56°C at approximately 5 bar pressure. Though this process is advantageous due to its reliance on proven technology and lack of chemical reagents, the capital and energy costs are quite high.

2.3.5. Summary of CO_2 capture technology: The CO_2 capture technologies described above are summarized in Table 2. Currently, MEA absorption is the industrially practiced CO_2 capture technology. However, current technology is only able to process 320-800 MT of CO_2 per day (coal-fired power plants produce ~1 MT_{CO2} MWh^{-1} or 12,000 MT of CO_2 per day for a 500 MW power plant)[117], which must be scaled to process the high volume of CO_2 that would be required to feed a solar refinery.[70] Alternative absorbents and other technologies (adsorption, membranes, and cryogenics) provide a number of advantages in terms of energy of separation, capital cost, mechanical robustness, chemical stability, and CO_2 capacity. Although, these technologies also present a number of issues that must be resolved. For adsorbents, the main challenge is to improve their stability and recyclability. Membranes have relatively low capital costs, but they require high partial pressure of CO_2 in order to have achieve high selectivity and high rates of separation. Therefore, there may be significant operating costs to compress the CO_2 stream. Similarly, cryogenic separation has high operating costs, and may be more viable from concentrated CO_2 streams. Specific cost estimates for some of these CO_2 capture methods are available (absorption[118-121], membranes[118, 122], cryogenics[118]), though they vary significantly depending on the assumptions employed, capacity, CO_2 concentration in the source, year of estimate, etc. Recently, Folger et al. reviewed commercial and pilot-scale demonstrations of these capture technologies, which utilize, almost exclusively, amine based absorption or physical absorption systems.[85]

Advances in fuel combustion technology[72, 73, 107] through oxy-combustion or IGCC, for example, may produce capture conditions which are suitable for alternative capture technologies. In particular, the high partial pressure of CO_2 in pre-combustion streams is more suitable for membrane separation or physical absorption/adsorption.

3. Hydrogen Production

The catalytic conversion of CO_2 to liquid fuels and chemicals requires the addition of hydrogen. Hydrogen is produced industrially using hydrocarbon feeds through three main routes: steam reforming of hydrocarbons (e.g. methane), partial oxidation, and autothermal reforming.[123] These reactions produce carbon monoxide, hydrogen and carbon dioxide. The amount and purity of hydrogen can be increased by water-gas shift and preferential oxidation of CO. NREL has calculated a levelized cost of hydrogen production from natural gas of 1.32 USD kg^{-1} (in 2005 USD), which achieves 71% process energy efficiency (using 2 MJ of process electricity per kilogram of hydrogen produced).[124]

Table 2. Assessment of various CO_2 capture strategies. Adapted from refs.[83, 125]

Technology CO_2 recovery	Material Capacity (g_{CO2} $g_{material}^{-1}$)	Conditions P(bar)/T(°C)	Energy Required (MJ kg_{CO2}^{-1})	Advantages	Disadvantages
Absorption 90-98%	MEA 0.4	1/40-60	4.0-6.0	• Mature process • Viable for low partial pressure of CO_2	• High cost for regenerating • Degradation • Challenge to scale up
Adsorption 80-95%			2.0-3.0		
	Zeolite 0.21	0.1-1/0-100		• High capacity • Stable • Fast adsorption kinetics	• Impurities affect selectivity
	MOFs 0.20	1/<100		• High surface area • High void volume • Tunable • Stable	• Recyclability not demonstrated
	Supported Amines 0.24	0.05-1/50-75		• Water tolerant • Fast adsorption kinetics • Viable for low partial pressure of CO_2	• Thermal degradation
	Metal Oxide 0.51	1/600-700		• High capacity • Inexpensive and abundant materials	• Low stability
	Hydrotalcite 0.29	1/500-600		• Stable	• Lower capacity than metal oxides
Membranes 80-90%	Polymer	15-20/100	0.5-6.0	• Simple • No reagents	• Requires high pressure • Low purity product • Thermal degradation
Cryogenic >95%			6.0-10.0	• No reagents	• High capital cost • High energy cost

In this section, we review methods of producing hydrogen from water using renewable, solar energy. The methods that will be discussed are electrolysis, photo-electrochemical water splitting, photo-catalytic water splitting, and thermochemical water splitting. For reference, the stoichiometry and thermochemistry of these processes are outlined in Table 3.

3.1. Electrolysis of Water

Electrolysis[126] uses electrical current to split water into hydrogen and oxygen, achieving hydrogen purity > 99.999%. Oxygen is evolved at the system anode, while hydrogen is evolved at the cathode. The overall process is endothermic, requiring a cell voltage of at least 1.23 V,

though, in practice, commercial electrolyzers require cell voltages around 1.9 V in order to overcome system inefficiencies and overpotential. The energy required for the electrolysis could be provided by solar-PV cells by connecting cells in series.[127]

Table 3. Reaction thermochemistry for water splitting reactions.

Reaction	Thermochemistry		
	$\Delta H°$ (kJ/mol)	$\Delta G°$ (kJ/mol)	E^0 (V)
$2H_2O \rightarrow 2H_2 + O_2$	483.6	457.2	1.19
$2H_2O(l) \rightarrow 2H_2 + O_2$	571.6	474.0	1.23

Table 4. Commercial water electrolyzer manufacturers and utilized technologies.

Company	Technology
Avalence	Alkaline
NEL Hydrogen	Alkaline
Proton OnSite	PEM
Teledyne Energy Systems	Alkaline
Hydrogenics	PEM
Industrie Haute Technologie	Alkaline

There are three main technologies for water electrolysis: alkaline electrolyzers, polymer electrolyte membrane (PEM) electrolyzers and solid-oxide electrolyzer cells (SOEC), details on the reaction chemistry for electrolyzers are provided in the supporting information. A survey of commercial electrolyzers shows that PEM electrolyzers are able to achieve system efficiencies of 56%, while the system efficiency of alkaline electrolyzers varies from 63-73%.[128] Commercial solar PV systems have demonstrated solar to electricity efficiencies in the range of 11.5-17.5%, and optimized PV-electrolyzer systems have achieved overall solar-to-hydrogen efficiencies of 12%.[129] A listing of commercial electrolyzer companies and their employed technologies are provided in Table 4. Capital costs for these systems have ranged from approximately \$400 to \$1600 per kg/day of hydrogen production capacity.[130] The levelized cost of hydrogen from electrolysis was calculated as 4.50 USD kg^{-1} (in 2005 USD) by NREL.[124]

3.1.1. Alkaline electrolyzers[126, 131] feature an aqueous alkaline electrolyte, ~30% KOH or NaOH and typically operate around 80-90°C, pressures up to 25-30 bar and require pure water (conductivity < 5 μS cm^{-1}). The cathodes are typically nickel coated with Pt, while the anodes are nickel with a metal oxide coating. Though, there have been efforts in developing more active, less-expensive, and durable electrocatalysts for hydrogen evolution (i.e. Ni alloys[132-134]) and oxygen evolution (i.e. metal oxides[135-137]).

Alkaline electrolyzers are commercially available as shown in Table 4. Unfortunately, there are some drawbacks to the technology, including crossover of hydrogen and oxygen through the semi-permeable diaphragm[138] and low current density due to high ohmic losses, thereby requiring large systems to produce high volumes of hydrogen.

3.1.2. Proton exchange membrane (PEM) electrolyzers[138-141] feature a thin (< 0.2 mm) cross-linked, perfluorosulfonic acid polymer membrane (e.g. Nafion) and precious metal electrocatalysts (e.g. Pt, Rh, Ir, Ru) on the electrodes. The conductivity of the polymeric

membrane restricts operation to below 100°C,[142, 143] but they can withstand high pressure, up to even 85 bar.[126] The water supplied must be even more pure than in the alkaline cell (conductivity $< 1~\mu S~cm^{-1}$).

PEM electrolyzers can be manufactured in a more compact design and have higher current densities than alkaline electrolyzers. Unfortunately, the membrane and precious metal electrocatalysts are expensive. Some possible alternative electrocatalysts for hydrogen evolution include metal carbides[144, 145], metal nitrides[144], while oxygen evolution electrocatalysts include metal (Ir, Sn, Ru) oxides.[146-150] Alternative electrolytes include solid acids, ceramic oxides, sulfonated aromatics, and heteropolyacids.[142, 151, 152]

3.1.3. Solid-oxide electrolyzer cells[126, 153-155] are high temperature (500-850°C), high pressure (30 bar) electrolyzers which feature a solid oxide electrolyte, typically yttria stabilized zirconia (YSZ). The cathode is often Ni-YSZ cermet, though precious metal catalysts are also active. The anode materials must be stable under highly oxidizing environments and are usually mixed oxide perovskites, e.g. lanthanum strontium manganite (LSM).[156-158]

The high temperature operation is advantageous because the *ΔG* of reaction decreases by 25% from 25°C to 1000°C, providing a significant electricity reduction for operation (though there is a cost to heat the water to the high temperature).[126] The electrical efficiency of SOEC systems has been reported to be as high as 85-90%.[159] In contrast, the mechanical robustness of the system is a challenge at high temperature operation.

3.2. Photo-electrochemical Water Splitting

Photo-electrochemical (PEC) water splitting[7, 160-165] follows similar principles as electrolysis, though the energy is supplied directly from light. In order to capture light, the anode, cathode, or both are made of a semiconductor material (referred to as a photo-electrode). A photo-anode is an n-type semiconductor; when a photon with energy greater than its band gap is adsorbed, an electron/hole pair is generated. The holes oxidize water to oxygen and the electrons travel through an external circuit to the cathode where hydrogen is evolved. A photo-cathode is a p-type semiconductor where water is reduced to hydrogen. In this case, oxygen evolution occurs on the counter electrode. Importantly, the photo-cathode or photo-anode must have a band gap which is at least as large as the thermodynamic potential, 1.23 eV. Though, in practice, due to energetic losses, a band gap of 1.6-2.0 eV is required.[123] Furthermore, the bottom of the conduction band must be more negative than the redox potential of H^+/H_2 (0 V vs. NHE) and the top of the valence band must be more positive than the redox potential of O_2/H_2O (1.23 V vs. NHE), see Figure 5. The most common material for the photo-anode is TiO_2. Even though it has a high band gap of 3 eV, its high corrosion resistance makes it an attractive material.[160] TiO_2 is typically paired with a Pt cathode.

Since TiO_2 has a wide band gap, it is unable to capture a majority of the solar spectrum (i.e. visible light). Therefore, it has a low solar to hydrogen efficiency of ~0.4%.[160] By assessing the energy lost per photon due to thermodynamic entropy of mixing and kinetic overpotential,

Murphy and co-workers suggested that an optimal material would have a band gap of 2.03 eV, which would correspond to a solar to hydrogen efficiency of 16.8% for AM1.5 solar irradiation.[166] Therefore, research has focused on identifying efficient, durable, and cheap photo-anodes and photo-cathodes for this reaction that maximize absorption of the solar spectrum. Promising photo-anode materials include metal oxides (doped-TiO_2[167, 168], WO_3[169, 170], $BiVO_4$[171-173], Fe_2O_3[174-176]), oxynitrides (TaON[177, 178], $LaTiO_2N$[179]), and GaAs-based materials.[180, 181] The conduction band levels of many of these visible light-active photo-anodes (WO_3, $BiVO_4$, Fe_2O_3) is too positive for hydrogen evolution because the O 2p valence band is very positive. This challenge can be overcome by applying an electrical bias to the system, though this lowers the overall energy efficiency of the system. Progress in the design of photo-cathodes has been less extensive, with promising materials including Cu_2O[182] and phosphides (InP,$GaInP_2$)[180]

Another method to increase the solar to hydrogen efficiency is to utilize a multijunction stack.[183] Multijunction stacks can be constructed using a combination of PEC and PV cells. The highest efficiency PV-PEC stack documented was developed at the National Renewable Energy Laboratory (NREL).[180] It is composed of a p-type $GaInP_2$ PEC cell connected to GaAs PV cell and has shown a solar to hydrogen efficiency of 12%.[180]

Recently, Nocera and coworkers developed an "artificial leaf," a triple-junction cell comprising earth abundant materials.[184] It consists of an amorphous silicon photo-voltaic interfaced to a Co-oxygen evolution complex (Co-OEC)[185, 186] and a ternary NiMoZn alloy hydrogen evolution catalyst. The technology was once being commercially developed by Sun Catalytix, though even with the use of cheap, earth abundant materials, the engineering cost was deemed too high for commercialization.[187] In particular, they estimated a hydrogen production cost of 6.50 USD kg^{-1}.

3.3. Photo-catalytic Water Splitting

Photo-catalytic water splitting[165, 188-191] follows the same principles as photo-electrochemical water splitting, though both oxygen evolution and hydrogen evolution occur on the same photo-catalyst, not separately on an anode and cathode, respectively. This simplifies the process, allowing powder photo-catalyst materials to be dispersed in water to evolve oxygen and hydrogen. Unfortunately, as a consequence of this, the separation of hydrogen and oxygen becomes more difficult. We briefly describe design considerations for photo-catalytic reactors in the supporting information.
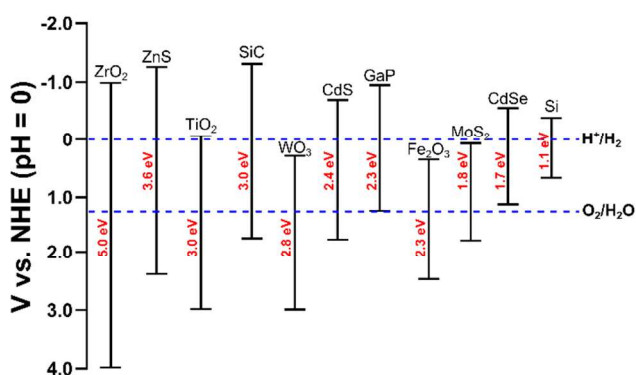
Figure 5. Band edges and band gaps for common semi-conductors and redox potentials for hydrogen and oxygen evolution reactions. Adapted from ref [188]

Photo-catalyst materials have the same band structure requirements as photo-electrodes. The photo-catalyst must have few defects, be highly crystalline, and have a short pathway for electron and hole migration to the surface. There have been a variety of different materials studied for photo-catalytic water splitting including metal oxides, oxysulfides, and oxynitrides.[188-191] Photo-catalyst particles are often accompanied by co-catalysts (e.g. metal nanoparticles) which are deposited onto the photo-catalysts. These provide active sites for the chemical evolution reactions with lower chemical barriers than on the semi-conductors.

However, even with all these materials tested, it is often difficult to find a material which absorbs visible light and has a conduction band level suitable for hydrogen evolution.[165] The state-of-the-art visible light active photo-catalyst, a solid solution of gallium and zinc nitrogen oxide ($Ga_{1-x}Zn_xN_{1-x}O_x$) with a mixed Rh-Cr oxide co-catalyst, only achieves a solar to hydrogen efficiency of 0.2%.[192, 193] One method to overcome this challenge, called the Z-scheme, involves splitting hydrogen evolution and oxygen evolution onto two different photo-catalysts which are connected via a shuttle redox couple (e.g. Fe^{3+}/Fe^{2+}, IO_3^-/I^-) in the solution.[194-196] This has the added advantage of separating the location of hydrogen and oxygen production, enabling easier separation. On the other hand, this system requires twice the number of photons as in the conventional system. Another recent method to utilize visible light is to incorporate plasmonic metal nanostructures (i.e. Au, Ag) into the photo-catalysts.[197]

3.4. Thermochemical Water Splitting

Solar energy can be collected and used for heat to thermochemically split water into hydrogen and oxygen. The direct thermolysis of water can be achieved at very high temperatures (> 2500 K). H-ion Solar Company developed a prototype nozzle/skimmer reactor system operating at 2600-2900 K which split water with 1-2% solar to hydrogen efficiency.[198] Though this is attractive due to its simplicity, reactor materials stability, difficulties in separating high temperature oxygen and hydrogen, and radiation losses made the system infeasible.[34, 199]

Alternatively, solar thermal energy can be used to drive a thermochemical cycle that have the net reaction of releasing hydrogen and oxygen.[6, 34, 199, 200] These "thermochemical water splitting cycles" usually consist of a high temperature endothermic reaction, followed by one or more exothermic steps.[34, 201] Over three hundred and fifty thermochemical water splitting cycles were investigated by the U.S. Department of Energy's Solar Thermochemical Hydrogen (STCH) program finding only nine that were deemed technically and practically feasible.[202] Accounting for the efficiency of the solar thermal collection system and the efficiency of the splitting reaction, the overall solar-to-hydrogen efficiency can approach 20%.[34]

High temperature (> 1000°C) thermochemical water splitting cycles usually consist of metal-oxide (e.g. Zn/ZnO[203], FeO/Fe_3O_4[204, 205], and others[206-209]) oxidation/reduction, generically:

$$MO_x \rightarrow MO_{x-\delta} + \delta/2 O_2$$

15

$$MO_{x-\delta} + \delta H_2O \rightarrow \delta H_2 + MO_x$$
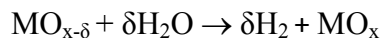
These oxidation/reduction cycles have several advantages: only two reaction steps reduces overall inefficiency and allows easy interfacing with the daily solar cycle (light on versus light off), hydrogen and oxygen are produced in separate steps, and separating the solid oxide from vapor product is simple.[34] An economic evaluation of a 100,000 kg_{H2} day^{-1} Zn/ZnO solar-thermochemical process estimated a hydrogen selling price of 5.58 USD kg^{-1} assuming that 70% ZnO conversion is possible.[210] Sandia National Laboratory has developed a CR5 reactor (counter-rotating ring receiver reactory recuperator) in which a cobalt ferrite/zirconia mixture is rotated through (1) a solar-irradiated high temperature receiver where it is reduced at 1400°C and then (2) a low-temperature hydrolysis reactor where hydrogen is evolved.[211-213]

Lower temperature thermochemical cycles are advantageous because there is less energy lost by radiation. One of the most promising is the sulfur-iodine (SI)[214, 215] cycle because of the low temperature (900-1000°C) required. Unfortunately, there are a number of drawbacks in this cycle. For one, H_2SO_4 must be separated from HI_x to prevent sulfur formation during HI decomposition. Furthermore, the separation of H_2 from HI and I_2 is challenging. Another promising method cycles between Mn(II)/Mn(III) oxides using a Na^{+} shuttle.[216] The main advantages of this approach are that the maximum temperature can be limited to 850°C and it does not involve any corrosive components. On the other hand, the $NaMnO_2$ must be cooled to 80°C in order to extract the Na^{+}, which may lead to overall high energy costs. Furthermore, the hydrogen must be separated from CO_2 (for pure hydrogen), requiring additional costs.

3.5. Summary of Solar Hydrogen Production Methods

The operating conditions, system efficiencies and advantages/disadvantages of these solar-based hydrogen production technologies are summarized in Besides these hydrogenation routes, CO_2 can also be converted to fuels using direct solar energy through electro-catalytic reduction, photo-electrochemical reduction, photo-catalytic reduction, and thermochemical reduction, as reviewed hereafter.

Table 5. Water electrolysis is a commercially demonstrated technology, and has reasonably high system efficiencies. Coupling with solar-PV technology is a near-term solution to producing clean hydrogen with reasonable solar to hydrogen efficiency. Photo-electrochemical and thermochemical methods are capable of achieving similar solar-to-hydrogen efficiencies as the electrolysis systems. Thermochemical cycles are more complex to engineer, have high radiative heat losses, and are capital intensive. Photo-electrochemical cells are only able to achieve these high solar efficiencies with complicated multi-junction systems which have been shown to degrade over time.[7] Photo-catalytic systems are attractive due to their simplicity, though current solar to hydrogen conversion efficiencies are very low due to low quantum efficiency and inability to harness visible light.[165] Additionally, separation of hydrogen and oxygen in these photo-catalytic systems remains an issue.

4. CO$_2$ Conversion

CO$_2$ can be converted to fuels using mature industrial processes with renewable, solar-derived hydrogen (as described in the previous section) and solar heat, as reviewed by Centi and coworkers.[1, 4] The reaction thermochemistry and stoichiometry for CO$_2$ hydrogenation reactions are shown in Table 6. In particular, the reverse-water-gas-shift reaction (RWGS) can be used to convert CO$_2$ and hydrogen to CO and water. The CO mixed with hydrogen produces syngas, which can be used to produce a variety of products, including methanol, dimethyl ether, or hydrocarbons through Fischer-Tropsch synthesis. There are also direct routes for hydrogenating CO$_2$ to products including methanol, methane, and formic acid.

Besides these hydrogenation routes, CO$_2$ can also be converted to fuels using direct solar energy through electro-catalytic reduction, photo-electrochemical reduction, photo-catalytic reduction, and thermochemical reduction, as reviewed hereafter.

Table 5. Summary of solar driven water splitting technologies.

System	Operating Conditions		System Efficiency	Solar-to-H$_2$ Efficiency	Advantages	Disadvantages
	P (bar)	T (°C)				
Alkaline Electrolysis	25-30	80-90	63-73%	10%*	• Commercial technology • Low capital cost	• Low current density • H$_2$/O$_2$ mixing
PEM Electrolysis	< 85	< 100	56%	8.5%*	• High current density • Compact design • H$_2$/O$_2$ produced separately	• High capital cost for membrane • Precious metal catalyst
Solid Oxide Electrolysis	30	500-850	85-90%†	12%*,†	• High electrical efficiency • Non-noble catalyst • H$_2$/O$_2$ produced separately	• Brittle ceramics
Photo-electrochemical	1	25	--	12%	• High solar efficiency • H$_2$/O$_2$ produced separately	• Degradation
Photo-catalytic	1	25	--	0.20%	• Simple process	• H$_2$/O$_2$ are mixed • Low solar efficiency
Thermolysis	1	2200	--	1-2%	• Simple process	• Low materials stability • H$_2$/O$_2$ are mixed • High radiative losses
Thermochemical	--	> 700	40%	18%‡	• High energy efficiency • H$_2$/O$_2$ produced separately	• High capital cost • Complex process design

* Assuming 15% solar PV efficiency
† Does not account for thermal energy
‡ Assuming 45% solar to thermal efficiency

Table 6. Reaction stoichiometry and thermochemistry for CO$_2$ conversion using solar-derived renewable hydrogen.

Product	Reaction	Thermochemistry	
		ΔH° (kJ/mol)	ΔG° (kJ/mol)
Carbon Monoxide	$CO_2 + H_2 \rightarrow CO + H_2O$	41.2	28.6

Methanol	$CO_2 + 3H_2 \rightarrow CH_3OH + H_2O$	-49.3	3.5
Methane	$CO_2 + 4H_2 \rightarrow CH_4 + 2H_2O$	-164.7	-113.3
Formic Acid	$CO_2 + H_2 \rightarrow HCOOH(l)$	-31.5	33.0

Table 7. Reaction stoichiometry and thermochemistry (equilibrium cell potential) for overall CO_2 reduction reactions using solar energy.

Product	Reaction	Thermochemistry		
		$\Delta H°$ (kJ/mol)	$\Delta G°$ (kJ/mol)	E^0 (V)
Carbon Monoxide	$CO_2 \rightarrow CO + 1/2O_2$	283.0	257.2	1.34
Formic Acid	$CO_2 + H_2O(l) \rightarrow HCOOH + 1/2O_2$	254.3	270.0	1.41
Formaldehyde	$CO_2 + H_2O(l) \rightarrow HCHO + O_2$	570.7	528.9	1.38
Methanol	$CO_2 + 2H_2O(l) \rightarrow CH_3OH + 3/2O_2$	764.1	706.1	1.23
Methane	$CO_2 + 2H_2O(l) \rightarrow CH_4 + 2O_2$	890.5	817.9	1.06
Ethylene	$2CO_2 + 2H_2O(l) \rightarrow C_2H_4 + 3O_2$	1411.0	1331.2	1.16

4.1. Electro-catalytic

The electro-catalytic reduction of CO_2[5, 217, 218] to fuels follows the same principles as electrolysis of water. Oxygen evolves at the cell anode, while CO_2 reduction occurs at the system cathode. The product of the reduction depends on the electro-catalyst used, and each of these products has a different thermodynamic cell potential, examples are indicated in Table 7.

Electrocatalytic reduction of CO_2 can be performed under ambient conditions using similar technology as water electrolysis.[219] The major obstacles to implementing this technology are catalytic in nature. That is, current electrocatalysts operate with high overpotentials, low faradaic efficiency (i.e. poor product selectivity), low current densities and are deactivated over time.[219, 220] Low faradaic efficiency occurs because the thermodynamic potential for CO_2 reduction is similar to that of water splitting (1.23 V), which allows for hydrogen evolution to compete with CO_2 reduction.

CO_2 electro-reduction has been studied over a variety of different catalysts[221], including metal complexes[222], transition metals[218], and metal oxides.[223] Of the metals studied, copper is the only one that is able to reduce CO_2 to hydrocarbons (i.e. methane, ethylene) with significant current densities at moderate overpotentials and reasonable faradaic efficiency.[224, 225] The major product is CO on Au, Ag, Zn, and Pd, it is $HCOO^-$ on Pb, Hg, In, Sn, Cd, and Tl, while it is hydrogen on Ni, Fe, Pt, Ti, and Ga. For CO_2 conversion to C_2H_4 on copper, the overall energy efficiency of the conversion is only 41% due to the high cathodic overpotential.[217] Furthermore, copper dissolutes in acidic environment and deactivation due to surface poisoning limit its efficacy.[219] Unlike on metal catalysts, CO_2 reduction on metal oxide catalysts (RuO_2[226] and copper oxides, in particular) has shown methanol to be a major product.[223, 227, 228] Other studies have shown that copper oxides have higher selectivity towards ethylene than pure copper.[224]

High-temperature CO_2 reduction has been demonstrated in solid-oxide electrolyzer cells.[153, 229] As with water electrolysis, the high temperature operation decreases the electrical energy required to drive the reaction, and the kinetics are also improved. Interest in this technology began in the 1960s by NASA in order to produce O_2 for life support and propulsion systems in

spacecraft.[230, 231] Recent work has focused on developing electrode materials for efficient CO_2 reduction to CO. Conventional Ni-YSZ electrodes are efficient for hydrogen evolution, but the activity is rather low for CO_2 reduction[229] and the stability is in question due to the formation of volatile Ni carbonyls.[232] One promising electrode material is ceramic $La_{0.8}Sr_{0.2}Cr_{0.5}Mn_{0.5}O_3$ (LSCM)[233], which has been combined with a Pd-ceria/YSZ co-catalyst to achieve efficient reduction of CO_2 at 800°C.[229] An extension of this technology is to perform high-temperature co-electrolysis of H_2O and CO_2 in a solid oxide electrolyzer cell to produce syngas at the cathode, and O_2 at the anode.[234-237] Graves et al. proposed a CO_2 to fuels process involving co-electrolysis, calculating that the process could operate at 70% electricity to liquid fuels efficiency.[238]

The majority of the literature on CO_2 reduction has been performed in batch systems with only a few reports for continuous operation for comparison.[239-243] Li and Oloman described a continuous, laboratory-scale CO_2 electro-reduction reactor which was able to achieve 20-80% conversion of CO_2 over a Sn-Cu catalyst with 6-17% organic product yield.[240] (This technology is being commercialized by Mantra Energy Alternatives, Ltd.) Xie and co-workers have developed a solid oxide electrolyzer operating at 614°C which has demonstrated CO_2 reduction to CO and CH_4 with a 60% conversion.[242] In the US, Liquid light Inc.[15, 244, 245] is commercializing an electrochemical process for conversion of CO_2 to chemicals such as ethylene glycol using proprietary catalysts.

4.2. Photo-electrochemical

The direct photolysis of CO_2 to CO and O_2 has been demonstrated using deep UV light (wavelength below 200 nm). Deep UV irradiation can be produced renewably using solar PV-powered low pressure mercury (185 nm) or deuterium (165 nm) lamps, at an energy requirement of 0.3 GJ mol^{-1}.[246, 247] Interestingly, CO_2 photolysis in the presence of hydrogen has demonstrated high selectivity to methane.[248] The hydrogen can be substituted with H_2O at the cost of lower CO_2 conversion due to competition with H_2O for photons.

The photo-electrochemical reduction of CO_2 follows the same principles as photo-electrochemical water splitting, as outlined in Section 3.2. As with water splitting, the main challenge is to find suitable photo-cathodes that allow for reduction using visible light irradiation. An additional complication, here, is that hydrogen evolution competes with CO_2 reduction. Therefore, there has been interest in using non-aqueous solvents for CO_2 photo-electrochemical reduction. Kumar et al. recently reviewed the state-of-the-art in photo-cathodes for CO_2 photo-electrochemical reduction in aqueous and non-aqueous solvents.[249] Some of the most common photocathode materials are p-Si[250], n-Si[251], p-InP[252, 253], p-GaP[254, 255], p-GaAs[256], n-GaAs[256, 257], and p-CdTe[253] with typical products: HCOOH, CO, CH_2O, and H_2. The product selectivity and activity can be altered by incorporating metal co-catalysts such as Au, Ag, Cu, Pd, Ni, Ru, Zn, In and Pb[250, 255, 258-260] or by covalently linking molecular catalysts to the surface.[261, 262]

4.3. Photo-catalytic

In 1979, Inoue and co-workers first reported photo-catalytic CO_2 reduction to HCOOH, CH_2O, CH_3OH, and CH_4 on powdered TiO_2, ZnO, CdS, SiC, and WO_3 under Xe lamp irradiation.[263] Since then, there have been investigations into a wide variety of materials, as recently reviewed.[8, 264] TiO_2 has been one of the most widely studied materials due to its durability, stability and lack of toxicity.[247, 265-272] However, due to its wide band gap, it is inactive under visible light irradiation, leading to low solar energy conversion. Doping TiO_2 (with e.g. Ag^{267}, Co^{273}, In^{274}, Cu-Fe^{275}, I^{276}, N^{277}) is one possible method to overcome this deficiency, while incorporating plasmonic nanoparticles is another attractive option.[197, 278] Aside from these thermodynamic limitations of TiO_2, other major challenges are catalytic in nature, namely low product selectivity, and low activity. To meet these challenges, metal co-catalysts have been incorporated into the photo-catalyst. Cu, Pd, Rh, Pt, and Au, added to TiO_2 has been shown to increase CO_2 conversion efficiency and selectivity. [266, 268, 279] In another report, Cu decreased selectivity towards CH_4, but lead to the formation of CH_3OH.[270] It has also been demonstrated that Hg improves the yield of CH_2O.[280]

4.4. Non-aqueous Reduction

A major challenge in these three CO_2 reduction technologies is that CO_2 solubility is low in the aqueous phase, which limits reduction rates. Additionally, hydrogen evolution from water competes with CO_2 reduction, lowering the solar-energy conversion efficiency. As a result of these two challenges, there has been interest in finding alternatives to aqueous phase reduction.

There have been a number of approaches to overcoming these main issues. Ogura demonstrated an electro-catalytic system where CO_2 is reduced selectively to ethylene at the three-phase (solid/liquid/vapor) interface of a metal-mesh electrode that is partially immersed in the solution. [225] In this way, CO_2 is directly supplied to the electrode from the vapor phase, overcoming much of the CO_2 transport issue. A similar, common, approach is to utilize gas-diffusion electrodes.[281-283] These porous electrodes are composed of hydrophobic materials which facilitates the formation of three-phase interfaces in the pores. Finally, non-aqueous solvents can be used in place of water. Some common examples include acetonitrile[284], methanol[285], dimethyl formamide[252], propylene carbonate[286], and ionic liquids.[287-289]

4.5. Thermochemical

One-step direct thermolysis of CO_2 to CO and O_2 is possible at extremely high temperature. At 3075°C, the reaction is thermoneutral[290], allowing for 100% conversion, but even a modest 30% conversion is possible at 2400°C.[291] Traynor and Jensen developed a prototype solar reactor, operating at 2400°, that achieved a peak solar to chemical energy efficiency of 5% with 6% conversion of CO_2.[292] Assessment of the technology indicates that a mature system may achieve up to 20% solar to chemical energy efficiency. Although these results are promising, the high temperature environment presents stability issues, radiative energy loss is high, and the high temperature CO/O_2 separation is a challenge.

These problems can be circumvented by employing redox thermochemical cycles, as similarly described for water splitting in Section 3.4. Two-step thermochemical cycles, in particular, are reasonably simple to implement, generate CO and O_2 in separate stages, and require lower operating temperature than direct thermolysis.[199, 293] Usually, these thermochemical cycles involve thermochemical reduction of a metal oxide followed by re-oxidation using CO_2 as an oxidant. Generically, the reaction proceeds as follows:

$$MO_x \rightarrow MO_{x-\delta} + \delta/2 O_2$$

$$MO_{x-\delta} + \delta CO_2 \rightarrow \delta CO + MO_x$$
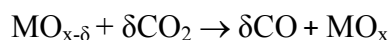
The Zn/ZnO thermochemical cycle is one promising technology, which has a theoretical maximum solar to chemical energy conversion efficiency of 39%.[291] The reduction of ZnO proceeds at 1600°C and re-oxidation by CO_2 occurs at 360°C.[294] One of the main drawbacks to this process is that the Zn is volatile and must be separated from O_2. Ferrites ($M_xFe_{3-x}O_4$) present another promising class of materials for thermochemical CO_2 splitting, though sintering, formation of liquid phases, and metal vaporization leads to loss of activity over cycling.[209, 295-297] A recent innovation is the so-called "hercynite cycle" in which a cobalt ferrite spinel ($CoFe_2O_4$) decomposes simultaneously with alumina (Al_2O_3) at 1460°C to form aluminates.[293, 298] Then, the alumina and cobalt ferrite spinel regenerate upon oxidation by CO_2 at 1000°C. This material has demonstrated stability over six thermochemical cycles without loss of surface area or activity.

Chueh et al. developed a prototype solar reactor utilizing a CeO_2-based thermochemical cycle to simultaneously split CO_2 and H_2O to produce CO, H_2 and O_2.[299, 300] CeO_2 reduction occurred between 1420-1640°C and oxidation at ~900°C, and the fuel production was stable over 500 cycles. The solar to fuel efficiency reached 0.8% with the majority of loss from thermal radiation and conduction, while theoretical assessment shows that 16-19% efficiency is possible.

Sandia National Laboratory have adapted their prototype CR5 reactor (as described in Section 3.4) for CO_2 splitting.[212, 213]

4.6. Summary of CO_2 Conversion Methods

Overall, there are a number of different routes and strategies for the conversion of carbon dioxide to fuels using solar energy as summarized in Figure 1. In one broad category, CO_2 is converted with hydrogen through mature industrial processes. The CO_2 can be converted directly using renewable-solar hydrogen, by RWGS with renewable hydrogen to produce syngas, or by solar-conversion of CO_2 to CO followed by reaction with renewable hydrogen (or WGS to generate the hydrogen). In a second broad category, CO_2 is directly reduced to fuel through PV-electrocatalytic, photo-catalytic, or photo-electrochemical methods. The former category is advantageous due to the maturity of the conversion methods, yet the simplicity of the conversion process in the latter category is attractive. However, compared with water splitting, the technology and catalysts for CO_2 reduction have been much less studied and remain much less efficient. In particular, conversion rates and selectivity are low.

5. Process Modeling and Analysis

In Sections 2-4, we summarized the state of key technologies involved in solar fuels production. In this section, we illustrate how these technologies are integrated into the solar refinery and critically assess what technological innovations are needed in order to develop a feasible process. Towards this goal, we employ process synthesis, modeling, and sensitivity analysis of possible solar refinery configurations. We consider two main cases based on the broad categories, (1) CO_2 conversion with hydrogen (Section 5.1) and (2) CO_2 reduction using water (Section 5.2). For the first case, we have developed a process model based on mature technology and evaluated the technical feasibility of the process based on an energy balance. For the second case, we first derive the mass balance for a generic solar CO_2 reduction process. Based on the mass balance, we have developed a generic energy cost model (that only examines the energy balance of this process) which can used to evaluate the energy feasibility of a solar CO_2 reduction process. These process models include not only reactant conversion processes, but also reactant acquisition (i.e. CO_2 capture), and separation processes. The separation steps are important for the overall process because of incomplete conversion of reactants, imperfect reaction selectivity issues, and the high energy requirements for some of these separations. The utility of the generic model is that it provides insight into how the various technologies in the solar refinery interact, and the extent to which changes to those individual technologies will affect the overall process mass and energy balances, as well as the process economics.

Later, we consider three simple case studies (Section 6) to demonstrate the use of the generic process model towards the production of methanol. Methanol was selected as the target product as it is one of the simplest liquid fuels and it can be converted to other chemicals or fuels using mature technologies. We note that this same framework can be easily modified to analyze other systems, or for the production of other fuels and chemicals. We perform a sensitivity analysis to develop targets for these technologies in order to achieve positive primary energy production (Section 7). Finally, we perform an economic assessment (Section 8), which allows us to determine the feasibility of the solar fuels technology and where future research should be focused.

5.1. Modified CAMERE Process for Methanol Synthesis from Solar-derived Hydrogen

In this section, we consider the production of methanol using mature technology with solar-derived hydrogen via a modified "carbon dioxide hydrogenation to form methanol via reverse-water gas shift reaction" (CAMERE) process.[12, 212, 301] A simplified block flow diagram of the process is shown in Figure 6. In the process, CO_2 is captured from a flue gas source (possible technologies are described in Section 2.3) and pumped to the facility. Hydrogen gas, produced using solar energy through one of the many different methods described in Section 3, is combined with CO_2.
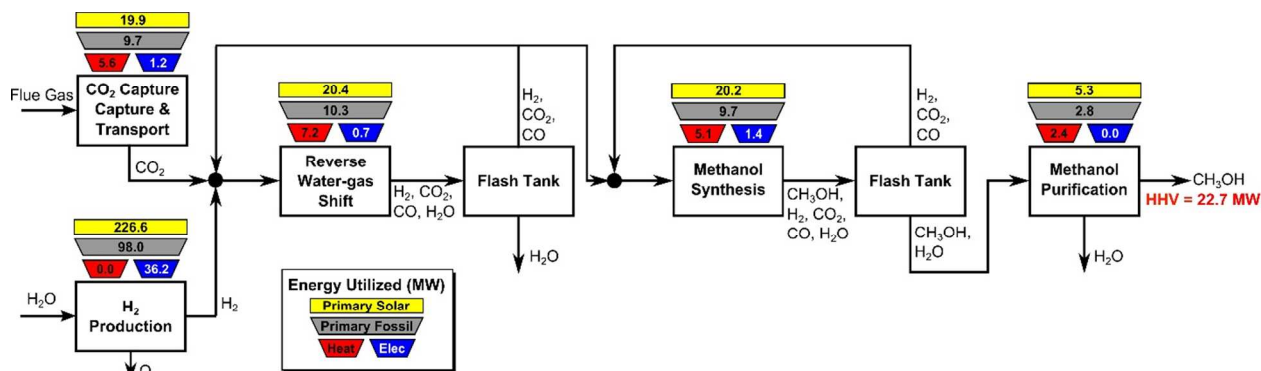
Figure 6. Block flow diagram for modified CAMERE process. The process heating (red trapezoids) and process electricity (blue trapezoids) are indicated for the major process blocks in units of MW. The higher heating value (HHV) of the methanol product is 22.7 MW. The process energy can be provided by fossil fuels or solar utilities (or a combination of both). If all fossil fuels are used, the required primary fossil fuel energy is indicated in the grey trapezoid above each block (assuming 86% fossil fuel to heating efficiency and 37% fossil fuel to electricity efficiency). Alternatively, if all the process energy is supplied from solar utilities, the required solar energy is indicated in the yellow square above each block (assuming 45% solar energy to heat conversion and 16% solar energy to electricity conversion). We do not provide numbers for the case where a mixture of fossil and solar utilities are used, in a given block.

The stream is compressed to 17 bar and heated to 320°C before entering the reverse water-gas shift reactor, in which CO_2 and H_2 are partially converted to CO and H_2O. The stream is cooled to 35°C to condense water which is removed in the flash tank, while a fraction of the vapor is recycled to increase overall CO_2 conversion and adjust the H_2:(CO+CO_2) ratio. The remaining CO, CO_2, and H_2 is compressed to 47 bar and heated to 206°C before entering the methanol synthesis reactor. The reactor effluent is cooled to 35°C and flashed to separate volatile CO, CO_2, and H_2, which are partially recycled to improve methanol yield, with the remainder discarded. The condensed methanol/water stream is expanded to remove residual incondensable material and then purified by distillation.

In Figure 6 the process energy (and equivalent primary energy) required for the main unit operations is reported, with a 1 kg s^{-1} (28,771 Mg yr^{-1} assuming 333 days per year operation) methanol production basis. In this case, the hydrogen production energy is calculated by assuming a 70% efficient alkaline electrolysis system (1.76 V cell voltage). We assume CO_2 is captured from flue gas. The energy required for this is assumed to be 3.1 MJ kg$_{CO2}$$^{-1}$ in process electricity and 0.7 MJ kg$_{CO2}$$^{-1}$ in process heat. (These numbers are based on Aspen simulations for MEA absorption.)

For a given process, energy is expended to move components, separate components, and convert species. In general, this process energy is derived from fossil fuels (i.e. primary energy). Conventional resources to electricity efficiency (η_E) ranges from 32-38% depending on the fuel mixture and we assume a value of 37% based on the following energy mixture (US 2011): coal (41%), natural gas (25%), nuclear (21%), petroleum (1%), and renewable (12%).[302] Natural gas to heat efficiency (η_H) varies from 85-90%, and we assume a value of 86%. If the process energy were provided by solar utilities, we calculate the solar energy required by assuming a 45% solar energy to process heat conversion efficiency[34] and a 16% solar energy to electricity conversion

efficiency (typical for crystalline silicon).[303] The goal of the process is to produce liquid fuel, which can be combusted to produce work or heating. We use the higher heating value (*HHV*) as a measure of its worth. For methanol, the *HHV* is 22.7 MJ/kg. For the process to be feasible, the primary fossil fuel energy consumed should be less than the heating value of the product. Therefore, we define the energy incorporation efficiency (*EIE*) as:

$$EIE = \frac{HHV_{product} - Total\ primary\ energy\ resources\ consumed\ (fossil\ fuels)}{HHV_{product}}.$$

In general, this efficiency varies from negative infinity to positive 100%. If the value is positive, the energy content in the fuel product is greater than the total fossil fuel energy expended. This is the feasibility point for our process and we refer to this as positive primary energy production. For clarity, at -100% energy incorporation efficiency, the primary energy consumed in the process is twice that of the heating value of the product.

We calculate the energy incorporation efficiency for three scenarios, as described hereafter and summarized in Overall, this analysis demonstrates that the modified CAMERE process described would only be energetically feasible if the hydrogen were produced using solar energy. Furthermore, even in this case, there must be improvements to reduce CO_2 capture costs or incorporate additional solar utilities into the process.

Table 8 and Figure 7. In Scenario 1, all process energy is provided by conventional fossil fuel utilities. The energy incorporation efficiency for the process is calculated as -477%. Examining the individual blocks in the flow diagram (Figure 6) it is clear that the energy cost for hydrogen production completely dominates the others. To illustrate this point, we consider a second scenario (Scenario 2) where all process utilities except for the hydrogen production system are provided by solar utilities. This scenario could also be thought of as the case where all other systems have been improved such that there is zero energy cost. Even in this extreme case, the energy incorporation efficiency would only increase to -332% because of the high energy cost for hydrogen production. Therefore, in order to achieve positive energy incorporation efficiency, hydrogen production must utilize solar-based technology (e.g. PV-alkaline electrolysis, photo-electrochemistry, photo-catalysis, thermal splitting). In Scenario 3, the energy of the hydrogen production system is provided by solar energy, while the energy for the other systems is provided by conventional fossil fuel utilities. However, even if all hydrogen production was via solar-energy, the energy incorporation efficiency would still be -43%.

Overall, this analysis demonstrates that the modified CAMERE process described would only be energetically feasible if the hydrogen were produced using solar energy. Furthermore, even in this case, there must be improvements to reduce CO_2 capture costs or incorporate additional solar utilities into the process.

Table 8. Primary energy source and energy incorporation efficiencies for modified CAMERE process scenarios

System Block	Primary Energy Source		
	Scenario 1	Scenario 2	Scenario 3
H₂ Production	Fossil	Fossil	Solar

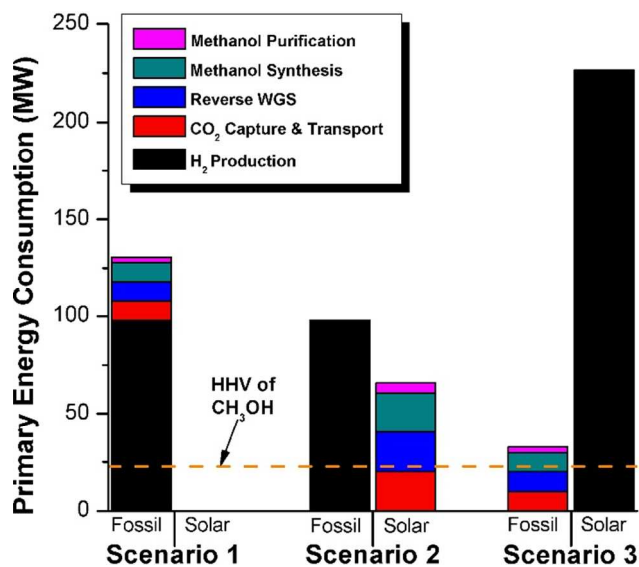|			
CO_2 Capture & Transport	Fossil	Solar	Fossil
Reverse WGS	Fossil	Solar	Fossil
Methanol Synthesis	Fossil	Solar	Fossil
Methanol Purification	Fossil	Solar	Fossil
Energy Incorporation Efficiency	-477%	-332%	-43%

Figure 7. Primary energy consumption for modified CAMERE process scenarios (1, 2, and 3) for 1 kg/s methanol production basis. The consumption of primary fossil and primary solar energy for each process system is indicated for each scenario. For comparison, the heating value of the methanol product is 22.7 MW, as indicated in the horizontal dashed orange line.

5.2. Generic Solar-driven CO_2 Reduction Process

In the previous section, we demonstrated that a methanol synthesis process from CO_2 could almost achieve positive energy incorporation efficiency if the hydrogen were produced using solar energy. An alternative to this process is to produce fuel directly from CO_2 and H_2O, without forming hydrogen as an intermediate product. Here, we present a generic process for CO_2 reduction by water to fuels, as shown in Figure 8. Possible technologies employed for this conversion were summarized in Section 4. In this reaction, the oxygen is removed as oxygen gas, which must be separated from the fuel product. We divide the generic process into five distinct sub-systems. In the CO_2 Capture & Transport sub-system (A), CO_2 is captured from some source (stream 1). The captured CO_2 is mixed with purified, recycled CO_2 (stream 9) and sent to CO_2 Reduction sub-system (B). Fresh water (stream 3) is mixed with recycled, purified water (stream 12) and fed to the CO_2 reduction sub-system. (In the generic process, we assume that no other solvents are used). In the CO_2 Reduction sub-system, CO_2 is reduced in a solar reactor to various fuel products with a one-pass CO_2 conversion of ξ. The one-pass water/CO_2 conversion is denoted by φ/ξ ($\varphi = \xi$ when there is a stoichiometric feed). The reaction stoichiometry is generically described by:

$$CO_2 + \upsilon_{H_2O}H_2O \rightarrow \sum_{i \in \mathbf{I}^V} \upsilon_i Z_i + \sum_{i \in \mathbf{I}^L} \upsilon_i Z_i + \upsilon_O O_2$$

25

with stoichiometric coefficients v_i and products Z_i. The sets $\mathbf{I}^V$ and $\mathbf{I}^L$ are subsets of $\mathbf{I}$ (the set of all species) which are vapor and liquid phase products, respectively. We will, in general, distinguish between vapor and liquid products because these two classes of products will be initially separated before further processing. (The vapor and liquid products are distinguished by their phases at standard conditions.) The carbon selectivity (S_i) for species i is defined as:
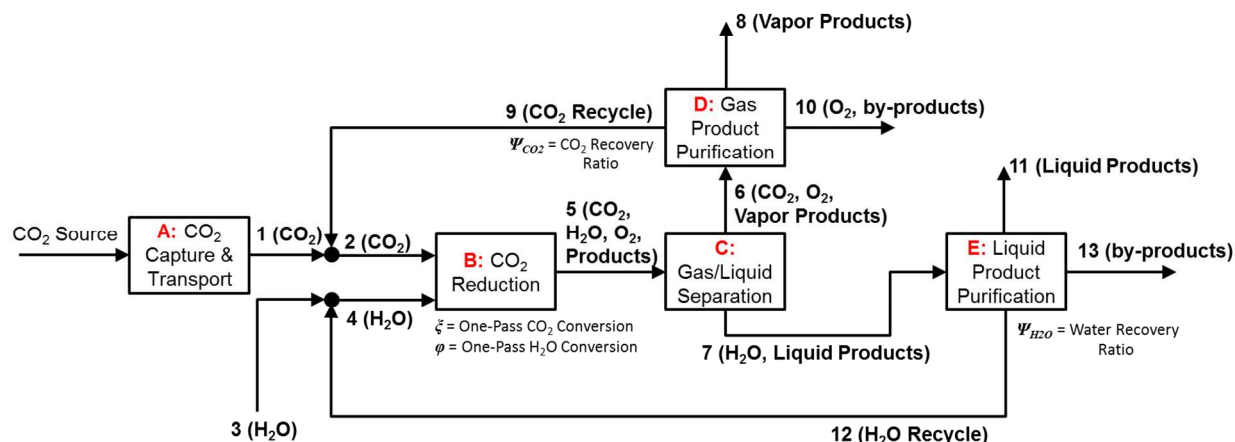

Figure 8. Block flow diagram for generic solar-driven CO_2 reduction process. Process variables indicated in the diagram.

$$S_i = \frac{N_{C,i} v_i}{N_{C,CO2} v_{CO2}}$$

where $N_{C,i}$ is the number of moles of carbon in one mole of species i. Since the stoichiometry of the reaction was written for 1 mole of CO_2, the denominator always equals 1. The products, unreacted H_2O and unreacted CO_2 exit the reactor (stream 5) and are separated into vapor (stream 6) and liquid (stream 7) streams in the Gas/Liquid Separation sub-system (C). The vapor is sent to the Gas Product Purification sub-system (D) where the desired products (stream 8) are purified from by-products (stream 10) and the CO_2 (stream 9) is separated and recycled. The ratio of the recovered CO_2 to the amount of CO_2 in entering the system in stream 6 is denoted by Ψ_{CO2}. The liquid from the Gas/Liquid Separation sub-system (stream 7) is sent to the Liquid Product Purification sub-system (E) where the desired products (stream 11) are purified from by-products (stream 13) and the unreacted H_2O is recycled (stream 12). The ratio of the recycled water to the unreacted water is denoted by Ψ_{H2O}.

In designing a CO_2 reduction process, there are a number of considerations including but not limited to: the source and method of CO_2 capture, the technology and catalyst employed for CO_2 conversion, and down-stream processing steps including methods of separating products from undesired by-products. A summary of the most important process considerations and options for each of the sub-systems are outlined in **Error! Reference source not found.**.

We note that both the gas and liquid product purification steps include only one product stream each (streams 8 and 11, respectively) and a single purge stream each (streams 10 and 13, respectively). In an actual process, there may be multiple liquid and multiple vapor phase

products (some desirable and others undesirable) that are separated into purified components (or lumped components) in these sub-systems. Stream 8 (and 11) represents the total mass of multiple product streams, each one purified to a desired specification. Similarly, stream 10 (and 13) represents the sum total of discarded materials. This includes purged materials to prevent build-up of components, separated undesirable by-products and mass losses due to imperfect separations (in particular CO_2 mass losses are included in the variable Ψ_{CO2}). In general, the separation blocks could be replaced with a purge (i.e. discarding a percentage of the materials without separating components). The advantage of such a scenario is that there is no direct capital or energy cost. However, indirectly, valuable product or reactants are lost, and the process must be scaled in order to reach a desired production basis. Also, since obtaining reactants requires energy (i.e. CO_2 capture), the trade-off may be sub-optimal, as we will demonstrate later. There may be no choice but to separate materials in order to meet a product specification. In a related note, in the generic process, we include recycle streams for the CO_2 (and also the water). Their existence is motivated by reported low conversions and the high cost for CO_2 capture (which must be significantly increased if un-reacted CO_2 is discarded). We will demonstrate the importance of the CO_2 recycle later.

Table 9. Process considerations and options for each of the process sub-systems.

Sub-System	Process Considerations and Options
A: CO_2 Capture and Transport	• What is the source of CO_2: atmosphere, post-combustion, pre-combustion, or oxy-combustion? • Which CO_2 capture technology should be employed (energy cost, capital cost)
B: CO_2 Reduction	• What solar reduction technology to use: PV-electrochemical, photo-electrochemical, photo-catalytic, or thermochemical? • What is the optimal catalyst: activity, product distribution (selectivity), and cost? • What are the reaction conditions: pressure, temperature, concentration of components (cell voltage)? • How should the oxygen by-product be handled? Can it be separated during reaction (i.e. separation of electrodes, Z-Scheme, etc.)? • How much catalyst should be used, what is the trade-off between capital cost of reactor and catalyst versus down-stream separation costs? • Should there be excess water or a solvent? How will product be separated from product? Is solubility of CO_2 in the solvent an issue?
C: Gas/Liquid Separation	• What are the components that need to be separated? • What is the best method for separating those components?
D: Gas Product Purification	• Are there desirable products and what are their purity specifications? • Should CO_2 be recycled and if so, what CO_2 separation technology should be employed?
E: Liquid Product Purification	• Are there desirable products and what are their purity specifications? • Are there any solvents or electrolytes that must be recovered?

5.2.1. Process model: Assuming idealized 100% separations (except for CO_2 and water recoveries) and no undesired by-products, we performed a mass balance on the entire system to determine how the size (mass treated) of the various units will vary with respect to the process variables ξ, φ, Ψ_{CO2}, and Ψ_{H2O} and reaction stoichiometry, v_{H2O}, v_{O2}, and v_i. The basis for the analysis is for X "value" in the product stream. In our model, we use the heating value of the product as our basis i.e.:

$$X = \sum_{i \in \mathbf{I}^P} F_{8,i} HHV_i + \sum_{i \in \mathbf{I}^P} F_{11,i} HHV_i$$

where $F_{j,i}$ is the molar flow rate of component i in stream j and the set $\mathbf{I}^P$ includes all product species which are deemed "valuable," i.e. undesired by-products are not included in this set. For a different basis, HHV could be replaced with another quantity (e.g. molecular weight for mass of product basis, molar volume for volume of fuel basis, etc.). We define the variable θ as:

$$\theta = \frac{X}{\sum_{i \in I^P} v_i HHV_i}$$

which describes how many moles/time of CO_2 must be consumed *in the reactor* to meet a given production basis, and it functions as a scaling factor the overall process (with units of moles/time). For a given value of X, the value of θ varies depending on the reaction stoichiometry and how each product is weighted. We then solved for the molar flow rates of the various species in each stream. The most important results are displayed in Table 10.

The mass of CO_2 that must be captured and transported to the solar refinery is a function of the amount of CO_2 consumed during the process. This includes the converted CO_2 as well as the amount lost during purification/processing. Since we assumed that the amount of recovered unreacted CO_2 is a fraction of the total amount unreacted, both the CO_2 conversion and recovery ratio affect the amount of fresh CO_2 that must be brought into the refinery. If all of the unreacted CO_2 were recovered ($\Psi_{CO2} = 1$) or all of the CO_2 were converted ($\xi = 1$), then $F_1 = \theta$, and is a constant (for a given process size). As a result, there will always be a cost associated with CO_2 capture and transport.

The fresh and recycled CO_2 and water streams enter the solar reactor and are converted to products. The feed streams (2 and 4) may need to be heated or compressed before entering the reactor. The amount of material processed is inversely proportional to their respective conversions. At 100% conversion, the amount of material is a constant value.

After conversion, the vapor and liquid products are separated. In the simplest case, this could be accomplished through a series of flash tanks. However, in general this may require more advanced separation technology to achieve reasonable separation, requiring heating and/or compression. The relative masses of the products (vapor, liquid, and oxygen) are constant for a given process basis, while the amount of water and CO_2 in the stream are functions of their respective conversions. Specifically, the amount of water and CO_2 is inversely proportional to their respective conversions, though at 100% conversion the amount reaches zero.

The gas product must be separated from CO_2 and O_2. The amount of product and O_2 are proportional to θ and their stoichiometric coefficients, while the amount of CO_2 varies inversely with the conversion. Therefore, the composition of the gas could vary significantly with conversion. At low conversion, CO_2 will be in high concentration, while at 100% conversion, there will be zero CO_2 in the stream. The optimal product/CO_2 separation strategy will likely

change with respect to this composition. Even in the case of 100% conversion, the product would still need to be separated from a constant amount of O_2. This could be avoided by choosing a CO_2 reduction technology where the CO_2 is reduced separately from oxygen evolution. This is possible by separating the anode and cathodes in electro-catalytic or photo-electrocatalytic systems. In photo-catalytic systems, separation of the two reactions has been demonstrated for water splitting (there, hydrogen evolution and oxygen evolution) using the Z-scheme, at the cost of solar efficiency.

Table 10. Molar flow rate in process streams shown in Figure 8, as functions of the process variables. If the flow rate of a component in a stream is not indicated, the value is zero. Streams 8-10 and 11-13 are derived from streams 6 and 7, respectively, based on the separation of the components in these streams into product, by-product, and recovery streams. For a given recovery of a component in those streams, the molar flow rate of that component in a stream can be readily calculated from the results for streams 6 and 7.

Stream	Molar Flow Rate
1	$F_{1,CO2} = \dfrac{\theta(1 - \Psi_{CO2}(1 - \xi))}{\xi}$
2	$F_{2,CO2} = \dfrac{F_{1,CO2}}{1 - \Psi_{CO2}(1 - \xi)} = \dfrac{\theta}{\xi}$
3	$F_{3,H2O} = \dfrac{\theta v_{H2O}(1 - \Psi_{H2O}(1 - \phi))}{\phi}$
4	$F_{4,H2O} = F_{2,H2O}\xi v_{H2O}\phi = \dfrac{\theta v_{H2O}}{\phi}$
5	$F_{5,CO2} = \dfrac{\theta(1 - \xi)}{\xi}, \quad F_{5,H2O} = \dfrac{\theta v_{H2O}(1 - \phi)}{\phi}, \quad F_{5,i \in I^P} = \theta v_i, \quad F_{5,O2} = \theta v_{O2}$
6	$F_{6,CO2} = \dfrac{\theta(1 - \xi)}{\xi}, \quad F_{6,V,i \in I^V} = \theta v_i, \quad F_{6,O2} = \theta v_{O2}$
7	$F_{7,H2O} = \dfrac{\theta v_{H2O}(1 - \phi)}{\phi}, \quad F_{7,i \in I^L} = \theta v_i$

The liquid product must be separated from water. The amount of product in the stream is proportional to θ and the stoichiometric coefficient. The amount of water is inversely proportional to the conversion of water, reaching zero at 100% conversion. Unlike the vapor product separation, there is not always an additional by-product (i.e. O_2) that must be separated. Though, for certain CO_2 conversion technologies, there may be additional components in the stream including electrolytes, other solvents, or other undesirable by-products that must be removed.

5.2.2. Energy model: We developed a simple energy cost model for this system. The overall process is composed of five sub-systems (with the total primary energy cost of the sub-system in parentheses), CO_2 capture & Transport (E_A), CO_2 Reduction (E_B), Gas/Liquid separation (E_C), Gas Product Purification (E_D) and Liquid Product Purification (E_E). The heating value of each product species, i in the subset of all valued product species $\mathbf{I}^P$ is given by HHV_i. Therefore, the energy incorporation efficiency (EIE) of the process is given by:

$$EIE = \frac{\sum_{i \in I^P}(HHV_i) - (E_A + E_B + E_C + E_D + E_E)}{\sum_{i \in I^P}(HHV_i)}$$

The energy function of these sub-systems depends on the specific technology being employed, the condition of the incoming streams, the specific components in those streams, and the mass of the components in those streams. For some systems, the cost may be proportional to the mass of a specific component. For instance, the cost of CO_2 capture from MEA absorption has been calculated to be proportional to the mass of the CO_2 captured.

We have developed energy cost functions for the five sub-systems in the generic process model, which are explained hereafter. In general, the energy cost for each sub-system, k, (E_k) was found to be proportional to the mass (volume) being processed by that sub-system. As a first approximation, the cost functions were written as the unit cost to process species i, multiplied by the flow rate of species i entering the sub-system in stream j ($F_{j,i}$):

$$E_k = \sum_{j \in J^k} \sum_{i \in I} F_{j,i} \left(\frac{W_{k,i}}{\eta_E} + \frac{Q_{k,i}}{\eta_H} \right)$$

where $W_{k,i}$ and $Q_{k,i}$ are the unit work and unit heating costs for species i in sub-system k and the set J^k is the set of all streams entering or leaving sub-system k. The unit cost parameters ($W_{k,i}$ and $Q_{k,i}$) can be evaluated through rigorous process simulations. In general, we note that lower-bounds for these energy costs could be estimated through simple minimum work calculations. We also note that many of these parameters could be approximated as zero.

6. Case study: CO_2 Reduction to Methanol Using Solar Energy

The generic framework that we developed in the previous section could be applied to analyze a variety of different systems. To illustrate this, we apply our generic process and energy models to a specific case: CO_2 photo-catalytic reduction to methanol with a methane by-product. Methanol (and methane) is produced directly, in a single-step, by photo-catalytic reduction of CO_2 based on results reported by Ikeue and co-workers using a Ti-containing porous silica photocatalyst.[304]

6.1. Process Model

We assume a CO_2 one-pass conversion of 5% with a methanol selectivity of 40% (methane selectivity 60%). Based on the selectivity, the reaction stoichiometry is as follows:

$$CO_2 + 2\,H_2O \rightarrow 0.6\,CH_4 + 0.4\,CH_3OH + 1.8\,O_2$$
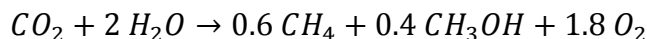
We assume the reactor is fed a stoichiometric CO_2:H_2O feed (implying that the water conversion is equal to the CO_2 conversion). We consider three case studies (we refer to these as Case I, II, and III to distinguish from previous Scenarios 1, 2, and 3), which are summarized in **Error! Reference source not found.**. Block flow diagrams of these process models are provided in the supporting information.

In Case I, CO_2 is captured from the dilute flue gas stream via MEA absorption and transported to the solar refinery. The CO_2 stream is mixed with water and heated to 50°C before entering the photo-reactor. In the solar-reactor, CO_2 and H_2O are converted using solar energy to methanol, methane and O_2. A series of flash tanks operating from 20 to 3 atm separate the vapor (CO_2, O_2, CH_4) from the condensables (CH_3OH, H_2O). The $CO_2/O_2/CH_4$ stream is vented, while the methanol is purified to 99.8% purity using a series of distillation columns with the water recycled (please see supporting information for more details). In Case II, the process is generally the same as Case I, except that unreacted CO_2 is recovered and recycled back to the solar reactor. The concentrated CO_2 in the vapor stream is separated by physical absorption using Selexol™[305, 306] and recycled to the solar-reactor. The CH_4/O_2 stream is vented. Finally, Case III is the same as Case II except that the initial CO_2 capture occurs from an oxy-combustion process through physical absorption using Selexol™.

6.2. Energy Model

The specific functional forms and unit cost parameters ($W_{k,i}$ and $Q_{k,i}$) for the generic energy cost functions were evaluated for the systems in the case studies using Aspen simulations (please see supporting information for specific details) and data from the literature, and are shown in **Error! Reference source not found.**. We caution that, in general, the energy costs that we derive from these simplified models are likely under-estimating the actual energy required for a given process.

The cost of the **CO_2 capture and transport sub-system (A)** was found to be proportional to the mass of the CO_2 captured:

$$E_A = F_{1,CO2}M_{CO2}\left(\frac{W_{A,CO2}}{\eta_E} + \frac{Q_{A,CO2}}{\eta_H}\right) = \frac{\theta M_{CO2}}{\xi}\left(1 - \Psi_{CO2}(1 - \xi)\right)\left(\frac{W_{A,CO2}}{\eta_E} + \frac{Q_{A,CO2}}{\eta_H}\right)$$

where $F_{1,CO2}$ is the molar flow rate of CO_2 captured, M_{CO2} is the molecular weight of CO_2, $W_{A,CO2}$ is the unit work required per mass of CO_2, and $Q_{A,CO2}$ is unit heating required per mass of CO_2. Based on Aspen simulations of the MEA absorption process, we have calculated values $W_{A,CO2} = 0.7$ MJ kg^{-1} and $Q_{A,CO2} = 3.1$ MJ kg^{-1}. For physical absorption using Selexol™, we use literature results for a 97% CO_2 recovery system, $W_{A,CO2} = 420$ kJ kg^{-1} and $Q_{A,CO2} = 0$.[307] We will refer to the term $\left(\frac{W_{A,CO2}}{\eta_E} + \frac{Q_{A,CO2}}{\eta_H}\right)$ as the "specific CO_2 capture cost".

The cost for the **CO_2 Reduction sub-system (B)** corresponds to reactor feed pre-heating, pumping and compression to the desired reaction conditions before entering the solar reactor. The heat and work required for these unit operations is assumed to be proportional to the mass flow rate of each of the components. Therefore, the energy cost function for the CO_2 Reduction sub-system is:

$$E_B = \sum_{i \in I} F_{2,i}M_i\left(\frac{W_{B,i}}{\eta_E} + \frac{Q_{B,i}}{\eta_H}\right)$$

where $F_{2,i}$ is the molar flow rate of component i in stream 2, M_i is the molar mass of component i, $W_{B,i}$ is the work required per mass of i and $Q_{B,i}$ is the heating required per mass of i. Assuming that the feed contains only CO_2 and water, we have evaluated the heat and work required to perform CO_2 reduction at 50°C and 1 atm. From Aspen simulation, we calculate $Q_{B,CO2} = 21.5$ kJ kg^{-1} and $Q_{B,H2O} = 104.1$ kJ kg^{-1}, with all other parameters equal to zero (assuming no pumping or compression is required). In reality, due to imperfect separations there may be other components in the stream which may need to be included in the energy cost function. We note that because solar irradiation may be directly used in the solar reactor, it is possible that the heating costs could be derived from this irradiation. Also, this does not account for the solar energy that is consumed in the actual chemical transformation.

Table 11. Case studies for CO_2 reduction to methanol with methane by-product. The technologies used in each sub-system are indicated along with the corresponding process and costing parameters for the mass and energy balances. For all cases: $\upsilon_{H2O} = 2$, $\upsilon_{CH3OH} = 0.4$, $\upsilon_{CH4} = 0.6$, $\boldsymbol{\upsilon_{O2}} = 1.8$, $\Psi_{H2O} = 1$, $\xi = 0.05$, $\varphi = 0.05$, and θ was set such that 1 kg/s of methanol is produced ($\boldsymbol{\theta} = (1\ kg/s)/(\upsilon_{CH3OH}M_{CH3OH})$), corresponding to a heating value of 22.7 MW. If not indicated, the parameter is equal to zero. All values are given in MJ kg^{-1}.

Sub-System	Case I		Case II		Case III	
	Technology	Process Parameters	Technology	Process Parameters	Technology	Process Parameters
A: CO₂ Capture and Transport	MEA absorption from post-combustion flue gas	$W_{A,CO2} = 0.7$ $Q_{A,CO2} = 3.1$	MEA absorption from post-combustion flue gas	$W_{A,CO2} = 0.7$ $Q_{A,CO2} = 3.1$	Physical absorption from oxy-combustion process	$W_{A,CO2} = 0.42$ $Q_{A,CO2} = 0$
B: CO₂ Reduction	Ti-SiO₂ Photo-catalyst.	$Q_{B,CO2} = 0.021$ $Q_{B,H2O} = 0.104$	Ti-SiO₂ Photo-catalyst	$Q_{B,CO2} = 0.021$ $Q_{B,H2O} = 0.104$	Ti-SiO₂ Photo-catalyst	$Q_{B,CO2} = 0.021$ $Q_{B,H2O} = 0.104$
C: Gas/Liquid Separation	Series of flash tanks	$W_{C,CO2} = 0.19$ $W_{C,O2} = 0.28$ $W_{C,CH4} = 0.55$	Series of flash tanks	$W_{C,CO2} = 0.19$ $W_{C,O2} = 0.28$ $W_{C,CH4} = 0.55$	Series of flash tanks	$W_{C,CO2} = 0.19$ $W_{C,O2} = 0.28$ $W_{C,CH4} = 0.55$
D: Gas Product Purification	None	$\Psi_{CO2} = 0*$	Physical absorption of CO₂	$\Psi_{CO2} = 0.97*$ $W_{D,CO2} = 0.42$	Physical absorption of CO₂.	$\Psi_{CO2} = 0.97*$ $W_{D,CO2} = 0.42$
E: Liquid Product Purification	Distillation	$m = 2.15†$ $b = -0.71*†$	Distillation	$m = 2.15†$ $b = -0.71*†$	Distillation	$m = 2.15†$ $b = -0.71*†$

* designates a dimensionless quantity

† the energy cost function for the distillation system is a more complicated power-law expression, see Section 6.2.

In the **Gas/Liquid Separation sub-system (C)**, the vapor and liquid components are separated for further processing. In the most simplified case, this could be accomplished through a series of flash tanks operating at different temperatures and pressures (see supporting information for the detailed process model for this system). Therefore, we have developed an energy cost function (E_C) that includes the energy required to compress and heat the various components, which is proportional to the mass flow rate of those components.

$$E_C = \sum_{i \in I} F_{5,i} M_i \left(\frac{W_{C,i}}{\eta_E} + \frac{Q_{C,i}}{\eta_H} \right)$$

where $F_{5,i}$ is the molar flow rate of component i in stream 5, M_i is the molar mass of component i, $W_{C,i}$ is the work required per mass of i and $Q_{C,i}$ is the heating required per mass of i. For the separation of CO_2, CH_4, and O_2 from CH_3OH and H_2O, the stream is compressed to 22 atm to condense residual water. Using a multi-stage compressor, the work required for each of the components was calculated as $W_{C,CO2} = 0.19$ MJ kg^{-1}, $W_{C,O2} = 0.28$ MJ kg^{-1} and $W_{C,CH4} = 0.55$ MJ kg^{-1}, respectively. The compression work could also be estimated by assuming ideal gas behavior. The reversible adiabatic work of compression for species X is given by:

$$W_{C,i} = \frac{\gamma R T_1}{M_i(\gamma - 1)}\left(\left(\frac{P_2}{P_1}\right)^{\frac{\gamma-1}{\gamma}} - 1\right)$$

where γ is the "heat capacity ratio", the ratio of the constant pressure heat capacity to constant volume heat capacity, T_1 is the initial temperature, P_1 is the initial pressure and P_2 is the final pressure. For the species considered here, the percent error in these ideal gas values are < 10% of the simulated results.

In the **Gas Product Purification sub-system (D)**, there are two main objectives. First, CO_2 should be separated and recovered for recycle. Second, any desirable vapor products should be purified to meet specifications. Purification of the vapor products may have a complicated functional form, and we do not provide a generic expression here. For our case studies, we are not interested in separating methane from oxygen, though we recover CO_2 for recycle. Therefore, we have defined an energy cost function (E_D) which is proportional to the mass of the CO_2 that must be separated as follows:

$$E_D = \frac{F_{6,CO2} M_{CO2} W_{D,CO2}}{\eta_E} = \frac{\theta(1-\xi)}{\xi\eta_E} M_{CO2}\left(\frac{W_{D,CO2}}{\eta_E} + \frac{Q_{D,CO2}}{\eta_H}\right)$$

where $W_{D,CO2}$ and $Q_{D,CO2}$ are the work and heat required per mass of CO_2. Assuming that the separation is via physical absorption in Selexol™, we again assume $W_{D,CO2} = 420$ kJ kg^{-1} and $Q_{D,CO2} = 0$.[307] We note that the cost could be reduced by lowering the CO_2 recovery ratio, but this would require additional CO_2 capture to balance the mass that is lost.

Finally, in the **Liquid Product Purification sub-system (E)**, desirable liquid products are purified and separated from unreacted water. For the specific case of methanol purification via distillation (see supporting information for detailed process model), the simple formulation used in the previous energy cost functions was unsuitable. Instead, we evaluated the energy cost (E_E) as a function of the weight fraction of methanol entering the distillation column and fit the data to a power-law (mx^b). The overall primary heating requirements for the separation is given by:

$$E_E = m\frac{F_{7,CH3OH} M_{CH3OH}}{\eta_H}\left(\frac{F_{7,CH3OH} M_{CH3OH}}{F_{7,CH3OH} M_{CH3OH} + F_{7,H2O} M_{H2O}}\right)^b = \frac{\theta m}{\eta_H}\frac{(v_{CH3OH} M_{CH3OH})^{b+1}}{\left(v_{CH3OH} M_{CH3OH} + \frac{(1-\phi)}{\phi} v_{H2O} M_{H2O}\right)^b}$$

where m and b were the results of the fitting, 2.15 MJ kg^{-1} and -0.71, respectively.

6.3. Model Results

Using these cost functions and the mass balances, we evaluated the primary energy expenditures in each of the five sub-systems for the three case studies as shown in Figure 9. The input parameters for the mass balances and cost model are given in **Error! Reference source not found.**. First, we note that all three cases have negative energy incorporation efficiencies, with Case I being the worst performer. Clearly, recycling unreacted CO_2 is of tremendous benefit. The reason for this is that the energy cost to produce 1 unit of CO_2 from dilute streams (i.e. via MEA absorption) is much higher than that from concentrated CO_2 streams (i.e. in the Gas Product Purification sub-system). Therefore, there will always be an energetic benefit of recycling CO_2 as long as the cost per unit is less than the initial cost of capturing CO_2. This simple calculation shows the importance of separations in terms of energy efficiency of the integrated process for solar fuels production. Comparing Case II with Case III, we see that changing the source of CO_2 (i.e. lowering the energy cost per unit of CO_2) has a significant effect on the overall energy efficiency, but the cost is relatively small compared with the energy costs for the other sub-systems. The reason for this is that the mass flow rates through the other sub-systems (B, C, D, and E) is much more strongly affected by CO_2 one-pass conversion. Since all of these cases are operating at relatively low conversion (5%), the energy costs for the other systems dominates. Interestingly, if we increase the CO_2 one-pass conversion, we find that neither Case I nor Case II is able to achieve positive energy incorporation efficiency even at 100% conversion. This is due to the high specific cost of CO_2 capture (see **Error! Reference source not found.**). In comparison, Case III achieves positive energy incorporation efficiency at 45% CO_2 one-pass conversion. We will revisit the sensitivity of the process to conversion in the Section 7.

7. Sensitivity Analysis of Case II

In this section, we build upon results from the previous case studies by performing sensitivity analysis on our Case II model (even though Case III had the most positive energy incorporation efficiency of the three cases studied), and will refer to it as the base case. We choose Case II as the basis because CO_2 capture from flue gas is easily retrofitted on existing power plants, and represents the most near-term solution for CO_2 capture. Therefore, unless otherwise indicated, the process parameters for the mass balance and energy balances are taken from that case.

7.1. Sensitivity to CO_2 One-pass Conversion

First, we evaluated the sensitivity of the process to changes in CO_2 one-pass conversion (ξ). The results of this analysis are shown in Figure 10. We caution the reader that since the original process was developed for low conversion, the optimal separation methods and technologies may change with conversion (or selectivity, later), which is not captured by our model.
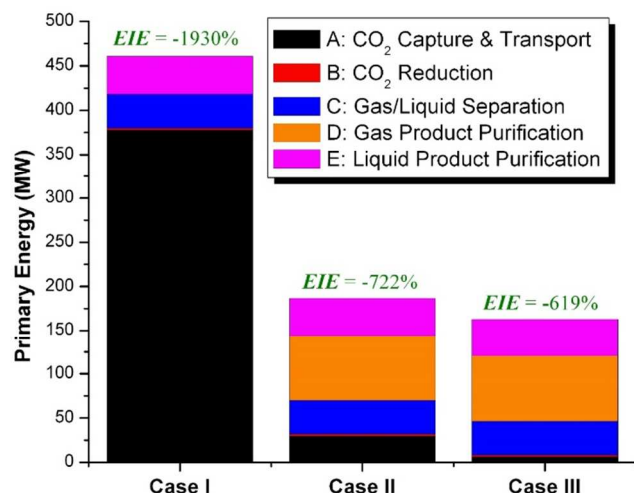
Figure 9. Primary energy expenditure for each sub-system for the three case studies. The heating value of the methanol product is 22.7 MW. The energy incorporation efficiency (*EIE*) for each case study is written above the respective bars.
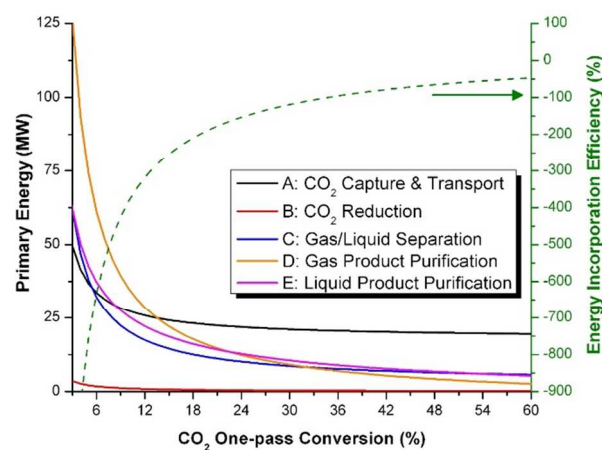

Figure 10. Primary energy costs for photo-catalytic reduction of CO_2 to methanol sub-systems as a function of CO_2 one-pass conversion with a 1 kg/s methanol production basis (22.7 MW HHV). Corresponding energy incorporation efficiency is plotted in green dashed line on the secondary y-axis.

First, one of the most important results of this analysis is the shape of these curves. The energy use scales inversely with conversion. Therefore, the energy incorporation efficiency improves as CO_2 one-pass conversion increases, at a decreasing rate (i.e. diminishing returns). Secondly, the results show that at low CO_2 conversion (<14%), the energy consumption in the Gas Product Purification sub-system is the most significant cost. In the base case for this sub-system, CO_2 is separated by physical absorption in Selexol™. The overall energy cost of this sub-system is high because (1) of the high specific cost of CO_2 separation, and (2) the mass being separated is inversely proportional to the conversion. Both of these effects contribute to very high total energy costs at low conversion. The next most significant costs are for methanol purification and gas/liquid separation, which also scale inversely with conversion. Above 14% one-pass conversion, the most significant energy cost is the CO_2 Capture & Transport sub-system. In the base case, CO_2 is captured from flue gas using MEA absorption. The energy cost decreases slightly with increasing CO_2 conversion due to fewer losses during separation, ultimately

35

plateauing at a cost of 18.9 MW at 100% CO_2 conversion (corresponding to 83% of the total heating value of the product). Therefore, even if CO_2 conversion could be improved by reaction engineering and catalyst design, it would be difficult to achieve positive primary energy efficiency without reducing the energy cost for CO_2 capture.

7.2. Sensitivity to CO_2 Capture Costs

As the CO_2 Capture & Transport sub-system represents the most significant energy cost at moderate to high conversion ($\xi > 14\%$), we have calculated the total primary energy cost (Figure 11) and energy incorporation efficiency (Figure S6) while also varying the specific CO_2 capture cost, $\left(\frac{W_A}{\eta_E} + \frac{Q_A}{\eta_H}\right)$. (For reference, the specific CO_2 capture cost for our simulated MEA absorption process is 5.5 MJ kg_{CO2}^{-1}).
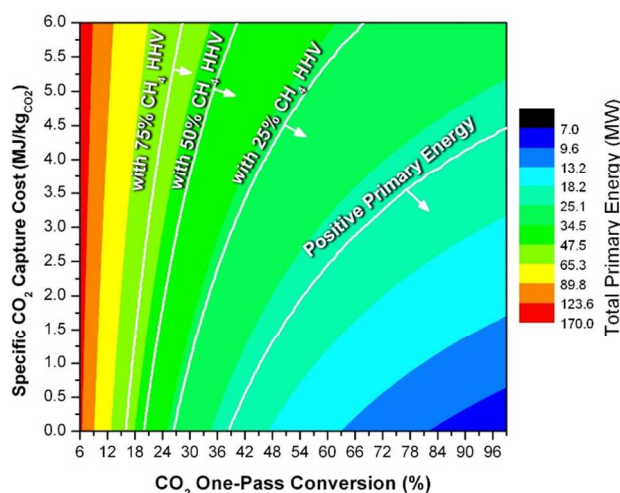

Figure 11. Total primary energy cost for photo-catalytic reduction of CO_2 to methanol process for 1 kg/s methanol basis (22.7 MW HHV) as a function of CO_2 one-pass conversion and specific CO_2 capture cost. A contour line for positive energy incorporation efficiency (22.7 MW primary energy cost) is indicated within and for positive energy incorporation efficiency while including the heating value of 25%, 50%, and 75% of the produced methane.

As we noted from the previous analysis, the CO_2 capture system encompasses a greater fraction of the overall energy cost with increasing CO_2 one-pass conversion. Furthermore, the energy cost for the CO_2 capture system asymptotes to a non-zero value quite rapidly with increasing CO_2 conversion. In particular, the energy cost is only 10% higher than its asymptote value at 33% CO_2 one-pass conversion. Therefore, at mid to high conversion, the overall energy cost for the system can be considered to be proportional to the specific CO_2 capture cost. These results manifest in Figure 11 by changes in the shape of the contour lines with conversion. At low conversion, improving CO_2 capture has an insignificant change in the primary energy efficiency, and the contours are nearly parallel with the CO_2 capture cost axis. At moderate and high conversion, the contour lines are sloped with respect to the CO_2 capture cost axis, and they can significantly affect the efficiency (even though the magnitude of the change in the cost is smaller at higher conversion).

If 100% conversion can be achieved, the specific CO_2 capture cost must be less than 4.4 MJ kg_{CO2}^{-1} in order to achieve positive energy incorporation efficiency, which is within the range reported in the literature (see Section 2.3). However, even if the cost of CO_2 capture were reduced to zero, a CO_2 conversion of 39% would be required. CO_2 capture costs as low as 0.5 MJ kg^{-1} have been reported for membrane separations, which would require a CO_2 conversion of ~42% to have positive primary energy production. Adsorption processes have been quoted in the 2-3 MJ kg^{-1} range, which require 54% and 69% conversion, respectively.

7.3. Sensitivity to Product Selectivity

As the CO_2 capture system represents one of the key energy costs in the overall process, reaction selectivity can be considered one of the main drivers for the overall cost. The reason for this is that by converting CO_2 to unwanted products, we not only waste the raw materials but we also waste energy to capture that material. However, if the by-product could be separated or combusted to provide process heating, the overall energy efficiency would improve. To quantify this effect, we first consider the case where the CH_4/O_2 stream is combusted to produce heat for the system. In **Error! Reference source not found.**Figure 11, we plot contours corresponding to positive primary energy production, with the inclusion of a fraction of the methane heating value (25%, 50%, and 75%). The plot shows that recovering even a small portion of the methane heating value can significantly reduce the required CO_2 conversion or capture costs. Additional details and discussion are provided in the supporting information.
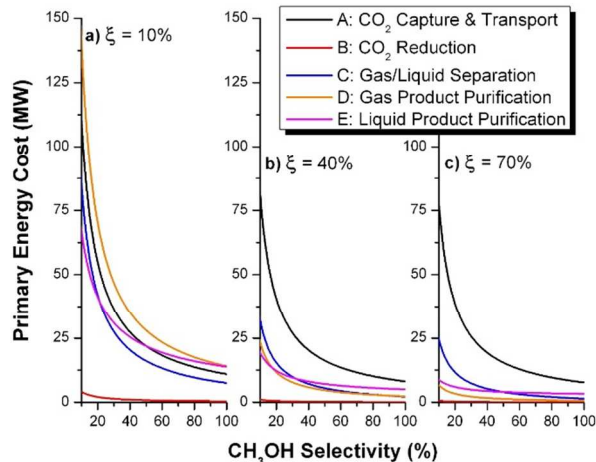
Figure 12. Primary energy costs for photo-catalytic reduction of CO_2 to methanol sub-systems as a function of CH_3OH selectivity with a 1 kg/s methanol production basis (22.7 MW HHV) for a) 10% CO_2 one-pass conversion, b) 40% CO_2 one-pass conversion, c) 70% CO_2 one-pass conversion.

An alternative to methane combustion is to develop a photo-catalyst (or alternative CO_2 reduction process) which is more selective for the desired product. In Figure 12 we plot the primary energy costs for the five main sub-systems as functions of methanol selectivity at 10%, 40%, and 70% CO_2 one-pass conversion. For our case, where only C1 species are produced, the carbon selectivity is equal to the stoichiometric coefficient, i.e. $S_{CH3OH} = v_{CH3OH}$. For a 1 kg/s methanol production basis, $\theta = (1\frac{kg}{s})/(S_{CH3OH}M_{CH3OH})$ and therefore one might conclude that the

molar flow rates of the streams should scale inversely with the methanol selectivity. For CO_2 and H_2O, this is true, and the costs follow the same dependence, as shown in Figure 12. Reactor heating costs are also proportional to water and CO_2 masses; inversely proportional to selectivity and the energy cost follows the same result. However, the dependence of methane and oxygen (and for alternative products, water as well) flow rates on selectivity is more nuanced. By mass balance, $v_{O2} = (4 - S_{CH3OH})/2$ and $v_{CH4} = 1 - S_{CH3OH}$. The corresponding flow rates are $F_{6,O2} = \theta v_{O2}$ and $F_{6,CH4} = \theta v_{CH4}$, respectively. Therefore, at low selectivity, they behave as if they scale inversely with selectivity, while at high selectivity they approach a non-zero constant value (since selectivity cannot exceed 1, none of the costs reach zero). In Figure 12, it can be seen that for a given CO_2 one-pass conversion, the relative ordering of energy costs for the sub-systems does not change with respect to selectivity, e.g. in Figure 12a CO_2 separation is the most costly regardless of selectivity. The main exception to this rule is the methanol purification system, which is a complicated function of selectivity. The cost of the purification varies with conversion, scaling as $S^{-0.71}$ at low water conversion and as S^0 (i.e. independent of selectivity) at high conversion (see supporting information).

Overall, due to these scaling relationships, the energy costs for all of the process sub-systems can be significantly reduced by improving reaction selectivity. If the selectivity were doubled from 40% to 80%, the cost of the CO_2 capture system, the reactor heating, and CO_2 separation would all be halved. Similarly, the energy cost for gas/liquid separation would be reduced by slightly more than 50%, while the energy cost for methanol purification would be reduced by slightly less than 50% (depending on the conversion).
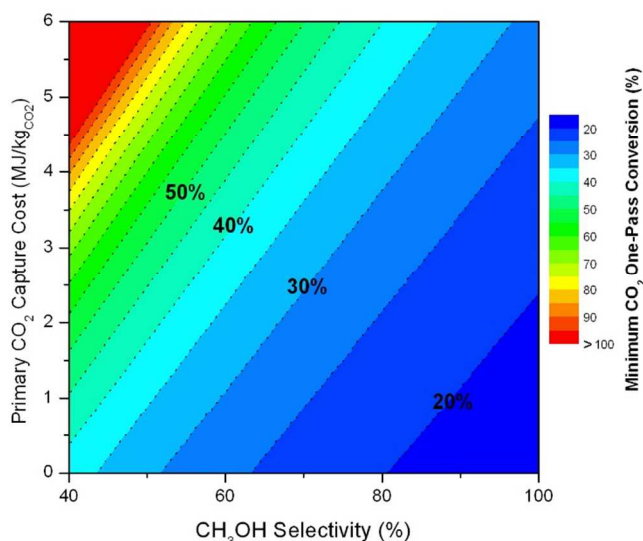
Figure 13. Minimum CO_2 one-pass conversion required to achieve positive energy incorporation efficiency as a function of methanol selectivity and specific CO_2 capture costs. Each contour line corresponds to a change in the minimum conversion of 5%. Since the maximum possible conversion is 100%, at high specific CO_2 capture costs and low methanol selectivity (upper left corner of contour plot) it is impossible to reach positive energy incorporation efficiency.

Finally, we consider the combined case where specific CO_2 capture costs are reduced and reaction selectivity improves. For a given specific CO_2 capture cost and reaction selectivity, we

calculated the minimum CO_2 one-pass conversion which would be required to achieve positive EIE. The results are shown in Figure 13. In order to achieve positive energy incorporation efficiency, a minimum of 15% CO_2 one-pass conversion is required. Beneath this value, even if the catalyst were 100% selective to the product, CO_2 would need to be supplied at a negative energy cost. If catalyst selectivity and CO_2 capture costs were improved by 25% with respect to the base case (i.e. 50% selectivity and 4.13 MJ kg_{CO2}^{-1} capture cost), the CO_2 conversion would need to be increased to 60% in order to achieve positive energy incorporation efficiency. With 50% improvement in both (60% selectivity and 2.75 MJ kg_{CO2}^{-1} capture cost) conversion would need to exceed 37%.

8. Economic Analysis

In our previous analysis, we demonstrated the application of a simplified energy cost model towards the development of improved solar to fuels processes. In that analysis, we did not account for the economic (operating and capital) costs. Importantly, the cost for the solar energy is completely discounted (i.e. free). Therefore, to understand the role of process economics and identify the major cost drivers, we developed a simple economic model for the estimation of a methanol minimum selling price (MSP). Based on discounted cash flow analysis (see Table 12 for major assumptions and supporting information for additional details), we calculated the MSP; i.e., the price of methanol that covers exactly all operating costs, income tax and return on investment. The utilities costs were scaled to the process (as a function of conversion, selectivity, etc.) using the generic mass balance and energy cost models as presented in the previous sections. For the base-case scenario, the cost to transport CO_2 and H_2O to the solar refinery would be 0.01 USD $kg_{methanol}^{-1}$ and 0.002 USD $kg_{methanol}^{-1}$, respectively, assuming 100 km transportation distances. Since these costs are quite low, we do not consider them in the model. We used a low-pressure steam price of 10.50 USD MT^{-1} and an electricity price of 0.06 USD kWh^{-1}.[308] The direct capital costs for all of the sub-systems were also scaled using the mass balances and the following equation:

$$Direct\ Cost(USD) = C_o \left(\frac{V}{V_o}\right)^{0.67}$$

where C_o is the direct capital cost calculated for a given mass flow through the system (V_o), and V is the mass flow through the scaled system. The direct capital cost for the CO_2 capture system and Selexol™ system were scaled using only the CO_2 mass flow rates, while the other scenarios were scaled with respect to the total mass flowing through the respective sub-system. Specific details of the capital costs for the five sub-systems, operating costs, and revenues are presented in the supporting information. All capital costs are scaled to a reference year of 2011 based on the Chemical Engineering Plant Cost Index (CEPCI).

First, we performed an economic evaluation of the base-case (Case II, see **Error! Reference source not found.**) while assuming that all costs (aside from the low-cost of pre-heating) associated with the CO_2 reduction sub-system were zero. The results of the economic evaluation

including operating costs, total project investment and minimum selling price are in Table 12. Major assumptions and parameters for economic evaluation.

Project economic life (yr)	30
Methanol production rate (Mg yr^{-1})	28,771
Rate of return (% per year)	8%
Tax rate (% per year)	35%
Depreciation method	Straight line

Table 13. For comparison, the industrial price of methanol fluctuates considerably, with a price of 0.632 USD kg$_{methanol}^{-1}$ in March 2014 (Methanex, non-discounted reference price in March 2014). The calculated minimum selling price is nearly 3 times higher than the industrial price, without including costs associated with the CO_2 reduction sub-system. As was described in the previous sections, the low conversion (5%) leads to large recycles and therefore high costs for utilities and capital.

Table 12. Major assumptions and parameters for economic evaluation.

Project economic life (yr)	30
Methanol production rate (Mg yr^{-1})	28,771
Rate of return (% per year)	8%
Tax rate (% per year)	35%
Depreciation method	Straight line

Table 13. Economic evaluation summary for Case II (see **Error! Reference source not found.**). All costs associated with the CO_2 Reduction sub-system are zero. For comparison, the costs are also provided in units of USD kg$_{methanol}^{-1}$ in square brackets. Mass balance parameters are as follows: $v_{H2O} = 2$, $v_{CH3OH} = 0.4$, $v_{CH4} = 0.6$, $v_{O2} = 1.8$, $\Psi_{H2O} = 1$, $\xi = 0.05$, $\varphi = 0.05$, and θ was set such that 1 kg/s of methanol is produced ($\theta = \frac{1\ kg/s}{v_{CH3OH}M_{CH3OH}}$).

Electricity (USD yr^{-1}) [USD kg$_{methanol}^{-1}$]	22,156,218 [0.77]
Low Pressure Steam (USD yr^{-1}) [USD kg$_{methanol}^{-1}$]	8,511,073 [0.29]
Fixed Operating Costs (USD yr^{-1}) [USD kg$_{methanol}^{-1}$]	10,279,745 [0.36]
Total Project Investment (USD) [USD kg$_{methanol}^{-1}$]	108,588,856 [0.13]
Minimum Selling Price (USD kg$_{methanol}^{-1}$)	$1.87

8.1. Sensitivity Analysis

Next, we performed sensitivity analysis on the process to understand how this impacts the economics. Here, we consider the effect of improvements to CO_2 one-pass conversion and methanol selectivity (with all other parameters given by the base-case scenario). In Figure 14a, we show the calculated minimum selling price of methanol as a function of CO_2 one-pass conversion and methanol selectivity. The point in the bottom left corner of the plot (5% CO_2 one-pass conversion and 40% methanol selectivity) corresponds to the base-case analysis, discussed previously. The results show that by increasing the one-pass conversion to ~12.5%, the minimum selling price of methanol can be halved from the base-case scenario. In contrast, the change in minimum selling price with respect to improvements in methanol selectivity are more modest. The selectivity would need to be improved to ~90% (at 5% CO_2 one-pass conversion) in order to halve the minimum selling price. In order to meet the industrial selling price of methanol,

0.63 USD kg^{-1}, the CO_2 one-pass conversion must be improved to 22% (without improving methanol selectivity). In contrast, by only improving selectivity, this price cannot be met. As we showed earlier, the process scales inversely with both conversion and selectivity, rationalizing the large improvements in process economics with small changes in conversion. Furthermore, this scaling explains why only modest improvements in minimum selling price can be accomplished by improving selectivity.

8.2. Solar Utilities

In the previous sensitivity analysis, we demonstrated how improvements in methanol selectivity and CO_2 one-pass conversion affect the minimum selling price of methanol. An important thing we did not consider in the previous analysis was the process energetics. In Figure 14a, we demarcate the process feasibility region, the region where the energy incorporation efficiency is non-negative. Interestingly, the minimum selling price of methanol is less than 0.30 USD kg^{-1} for all points (selectivity, conversion) in this region. As the goal is to produce methanol at a competitive price, with positive energy efficiency, and with minimum improvements in process technology, we can afford to expand the feasibility region outward (to lower conversion and selectivity) by trading monetary costs for energy costs by employing solar utilities.

In our original economic analysis, we used fossil fuel utilities prices of 0.060 USD kWh^{-1} for electricity and 10.50 USD MT^{-1} (~0.017 USD kWh^{-1}) for process steam. In comparison, the levelized cost of solar-PV electricity has been studied quite extensively, and we will assume a value 0.144 USD kWh^{-1}.[56] In contrast, the cost of solar process heating has not been studied as extensively, we will use a literature value of 0.05 € kWh^{-1} (0.069 USD kWh^{-1} assuming a 1.38 USD to 1€ exchange rate).[309] Based on these prices, we found that is more economical to first replace fossil fuel heating with solar heating, and then replace fossil fuel electricity with solar-PV electricity, see the supporting information for more details.

With this result, we revisited the selectivity study from the previous section and re-calculated the minimum selling price as a function of methanol selectivity and CO_2 one-pass conversion. However, we allowed for solar utilities to be used in addition to fossil fuel utilities, and imposed the constraint that the energy incorporation efficiency is non-negative. The results are shown in Figure 14b. Based on the assessment of cost of primary energy avoidance, at each point in the plot (selectivity, conversion) the minimum selling price is achieved by first replacing fossil fuel-derived electricity with solar electricity and then fossil fuel-derived heating with solar heating until the energy incorporation efficiency becomes non-negative. For regions in the phase-space where the conversion and selectivity are both low, energy costs present a high fraction of the overall costs (please see supporting information for cost distribution) and therefore replacing those with solar utilities greatly increases the minimum selling price (see inset of Figure 14b). For example, for the base-case scenario (5% conversion, 40% selectivity), the MSP of methanol increases from 1.87 USD kg^{-1} to 3.39 USD kg^{-1}. If the CO_2 one-pass conversion increases (with 40% selectivity fixed), the industrial price of methanol (0.63 USD kg^{-1}) is achievable at 38%

conversion, whereas with just fossil fuels utilities, this is reached at 22% conversion (the MSP with solar utilities is 0.97 USD kg^{-1} at 22% conversion and 40% selectivity).
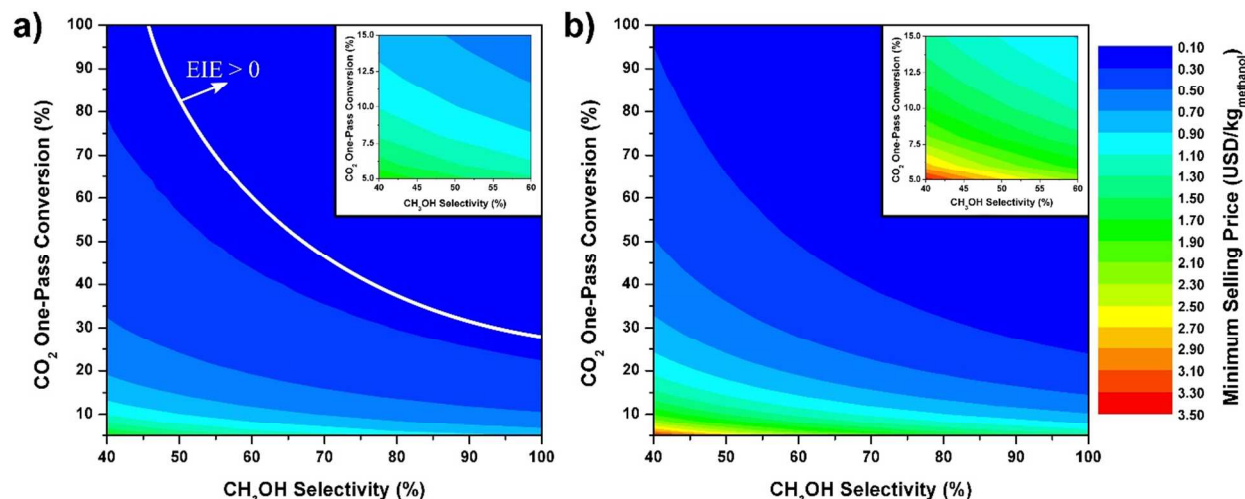

Figure 14. (a) The minimum selling price of methanol (USD kg^{-1}) for base-case scenario with improvements in methanol selectivity and CO_2 one-pass conversion. The upper right region, demarcated with a white line, shows the conditions (selectivity and conversion) that achieves positive energy incorporation efficiency. **(b)** the minimum selling price of methanol (USD kg^{-1}) calculated as in a), but the conventional fossil fuel utilities are replaced with just enough solar utilities such that the energy incorporation efficiency is non-negative at all points in the phase-space. The inset of each plot shows the low-conversion and low-selectivity region with higher resolution (40-60% CH_3OH selectivity, 5-15 % conversion). All capital and energy costs associated with the CO_2 reduction (B) sub-system are set to zero.

8.3. CO$_2$ Reduction Sub-system

In the previous economic analyses, operational and capital costs associated with of the CO_2 reduction sub-system were omitted. The reason for this omission is that there are a wide variety of technologies available for CO_2 conversion and types of solar reactor architectures, as well as limited available literature on continuous processes. For a specific CO_2 reduction process, the minimum selling price for methanol (or a different product) can be found by calculating the levelized cost of that specific system with respect to the amount of product produced (i.e. cost per unit produced) and adding that value to the calculated MSP from the previous section(s), which is a function of CO_2 one-pass conversion, product selectivity, and solar energy utilization. To demonstrate this procedure and provide some benchmarks of costs for this sub-system we consider two simplified cases that are meant to illustrate the state of the technology. First, we consider the case of CO_2 electro-reduction using PV-solar electricity. In the second case, we consider CO_2 photo-catalytic reduction.

The equilibrium cell potential for CO_2 electro-reduction to methanol is 1.23 V, see Table 7. Assuming 100% selectivity (no energy is wasted to produce by-product) and 100% electrolyzer efficiency (i.e. no overpotential losses), 22 MW of electricity is required to produce 1 kg/s of methanol. Using a levelized cost of solar electricity of 144.3 USD MWh^{-1} from the literature,[56] the cost of the PV-solar electricity is 0.88 USD kg$_{methanol}^{-1}$ (corresponding to a capital cost of $759,554,400). Therefore, the MSP of methanol would be at least 0.88 USD kg$_{methanol}^{-1}$ more

42

than is indicated in Figure 14, at every point (though this value would be under-estimating the electricity cost at lower selectivity). (We note that, assuming 6 kWh m^{-2} average daily incidence with 16% solar to electricity conversion (typical for crystalline silicon),[303] this would require 551,562 m^2 (136 acres) of incidence area). In comparison, the levelized cost of electricity from a natural gas-fired conventional combined cycle is 67.1 USD MWh^{-1}.[56] Therefore, if the electrolyzer were powered by natural-gas energy, the minimum selling price would be increased by 0.55 USD kg$_{methanol}^{-1}$. More realistically, CO_2 electro-reduction to methanol has been demonstrated with ~60% faradaic efficiency at -0.8 V$_{SCE}$ on RuO_2 electrodes.[226] Including an additional assumed 0.5 V oxygen evolution overpotential, the overall electricity cost would be 66 MW, or 2.64 USD kg$_{methanol}^{-1}$ for the solar-PV electricity. We note that this does not include costs associated with the actual electrolyzer unit or any electrocatalysts. As the cost of solar electricity completely dominates the overall process cost, improvements in PV technology would be paramount towards achieving a low minimum selling price. Additionally, improvements in electrocatalyst performance through high faradaic efficiency and low overpotentials would have a tremendous effect on the economics.

Photo-catalytic systems may have lower costs for the solar energy because it does not need to be converted into electricity. However, reported photo-catalytic reaction rates are very low, on the order of ~0.1-10 μmol$_{product}$ g$_{cat}^{-1}$ h^{-1}.[8, 304, 310, 311] In contrast, methanol synthesis rates on commercial $Cu/Zn/Al_2O_3$ catalysts (498 K, 50 bar, gas hourly space velocity (GHSV) = 10000) range from 0.3-1.5 kg$_{methanol}$ L$_{cat}^{-1}$ h^{-1} (using a bulk catalyst density of 1.2 g cm^{-3}, the rates are 7800-39000 μmol g$_{cat}^{-1}$ h^{-1}).[312] As a result, though the cost of the solar energy may be lower, the cost of the photo-catalyst will be quite significant. Assuming a catalyst activity of μmol$_{product}$ g$_{cat}^{-1}$ h^{-1} and that the required amount of photo-catalyst scales linearly to meet the 1 kg s^{-1} methanol production rate, 1.1 x 10^8 kg of TiO_2 catalyst would be required. At a price of 1 USD kg$_{TiO2}^{-1}$, assuming a catalyst lifetime of one year, the additional operating cost would be 3.91 USD kg$_{methanol}^{-1}$ ($112,500,000 yr^{-1}), thereby increasing the minimum selling prices reported in Figure 14 by 3.91 USD kg$_{methanol}^{-1}$. At a more ambitious catalyst lifetime of 10 years, the additional operating cost would still be 0.39 USD kg$_{methanol}^{-1}$. Though these parameters could be off by ~1 order of magnitude, the calculated cost serves to illustrate the importance of improving the photo-catalytic activity towards developing an economical process.

To assess any other CO_2 reduction process, if the levelized cost of the CO_2 reduction sub-system were known (or calculated), the minimum selling price of methanol (or some other product) could be calculated by adding that levelized cost to the minimum selling price shown in Figure 14a or Figure 14b (depending if solar utilities will be used).

9. Summary and Outlook

In this publication, we reviewed the state of the art in solar conversion of carbon dioxide to fuels and demonstrated two conceptual processes for the production of methanol using these technologies. In the first example, we showed how the energy efficiency of mature CO_2 conversion processes could be significantly improved by utilizing solar-derived hydrogen for

Energy & Environmental Science

hydrogenation. The current state of water-splitting technology is significantly more advanced than analogous CO_2 reduction technology, with solar to hydrogen efficiencies > 10% achievable. Therefore, this presents a promising near-term method for leveraging solar resources. In the second example, we considered the case of a one-step, solar CO_2 reduction with H_2O process where methanol and methane are produced (with oxygen). We developed a generic cost model for the process and applied the model to a methanol production process by using results from simulation and the literature. We performed sensitivity analysis to determine the influence of different process parameters (i.e. conversion, selectivity, and CO_2 capture energy costs) on the energy efficiency of the process.

One-pass CO_2 conversion and carbon selectivity have dramatic effects on the overall process energy efficiency. As a first approximation, the amount of material flowing through the various sub-systems is inversely proportional to both of these parameters. Therefore, improving both of these through reaction engineering and catalyst design will be essential towards achieving high primary energy efficiency (and low capital costs). Thus, reactions that can only obtain low one-pass CO_2 conversion are likely to never be economically beneficial and will always require more energy than they produce because of the high energy costs to recover/recycle CO_2 and to separate the products from the oxygen and unreacted H_2O. As the selectivity and one-pass conversion increase, the marginal improvement on energy incorporation efficiency diminishes. Additionally, CO_2 capture presents an essential area for research. The energy required for CO_2 capture via MEA absorption from dilute flue gas currently accounts for ~80% of the total energy of the methanol product at 100% CO_2 one-pass conversion and 40% methanol selectivity. Therefore, even with dramatic improvements in conversion and selectivity, it will be impossible to achieve 100% primary efficiency without significant improvements to the technology. Efforts in developing solid adsorbents, membranes, or by capturing from more concentrated CO_2 streams (pre-combustion or oxy-combustion capture) could decrease energy cost of CO_2 capture. We calculate that if the energy cost of CO_2 capture were reduced by 50% and the selectivity of the catalyst were improved by 50% (to 60% methanol selectivity), the minimum CO_2 one-pass conversion to achieve positive energy incorporation efficiency is 37%.

Through a simplified economic analysis, we calculated the minimum selling price for methanol as a function of the methanol selectivity and CO_2 one-pass conversion, assuming, first, that the capital and operating costs for the CO_2 reduction sub-system were all zero. For the base-case scenario (40% selectivity and 5% conversion), we find a minimum selling price of 1.87 USD $kg_{methanol}^{-1}$, which is approximately three times the industrial selling price. The minimum selling price can be reduced to the industrial price by improving CO_2 one-pass conversion to 22% (with 40% selectivity). However, we find that even if the industrial selling price can be met, the energy incorporation efficiency would still be negative. In fact, the process must be improved (selectivity and conversion) such that the minimum selling price is less than 0.30 USD $kg_{methanol}^{-1}$ for the energy incorporation efficiency to be non-negative. Since this price is below the industrial selling price, one can afford to trade increased costs, by purchasing solar utilities to replace fossil fuels utilities, for improvements in overall energy incorporation efficiency. This expands the

feasible region to lower selectivity and conversion. To meet the industrial selling price with non-negative energy incorporation efficiency, the conversion must be improved to 38% (with 40% selectivity).

To assess the costs of the CO_2 reduction sub-system, we considered two simplified cases: (1) CO_2 electro-reduction and (2) photo-catalytic reduction of CO_2. Based on current estimates, even at 100% faradaic efficiency and no overpotential, the cost of the solar electricity to power the electrolyzer is 0.88 USD $kg_{methanol}^{-1}$, (increasing the minimum selling price by 0.88 USD $kg_{methanol}^{-1}$ from the results of the previous analyses). This does not even include costs associated with the electrolyzer, itself, or any electrocatalysts. To compete with the industrial methanol selling price (0.632 USD $kg_{methanol}^{-1}$ in February 2014), the cost of solar electricity would need to be decreased dramatically (over 50%). While photo-catalytic systems would benefit from reduced solar energy costs (non-electrical), photo-catalytic activities are very low, on the order of ~1 µmol g_{cat}^{-1} hr^{-1}, which presents an even higher catalyst operating cost of 3.91 USD $kg_{methanol}^{-1}$ (assuming 1 year catalyst lifetime) This does not include the cost of the solar reactor, which would need to be massive (on the order of 10^5 m^3) to contain all of the photo-catalyst. Therefore, the activity of the photo-catalyst would need to be improved by several orders of magnitude.

As we move towards more sustainable energy resources and try to reduce our dependence on fossil fuel reserves, our society is faced with one of the biggest technological challenges of solar energy conversion. With a concerted collaborative effort among researchers from the fields of chemical engineering, material science, physics, chemistry; we can realize our goal of a sustainable carbon based energy economy. Modeling and analysis of these solar fuels processes would play a pivotal part in the development of these technologies.. By reviewing the state of the art technologies in the field and identifying key areas of future research through conceptual process design, we hope that our study helps accelerate the growth of solar fuels processes towards commercialization.

Nomenclature

Sets

$i \in I$	Species
$j \in J$	Process streams
$k \in K$	Process sub-systems

Subsets

I^L	Liquid phase product species

I^P	*Valued* product species
I^V	Vapor phase product species
J^k	Process streams entering sub-system k

Parameters

b	Power law exponent for energy cost of distillation system
C_o	Direct capital cost of reference equipment
E_k	Total primary energy cost of sub-system k
EIE	Energy incorporation efficiency
$F_{j,}$	Total molar flow rate in process stream j
$F_{j,i}$	Molar flow rate of species i in process stream j
HHV_i	Heating value of species i
m	Power law coefficient for energy cost of distillation system
M_i	Molecular weight of species i
n	Total moles
$N_{C,i}$	Moles of carbon in species i per 1 mole of species i
P	Pressure
$Q_{k,i}$	Unit heat required for sub-system k to process species i
R	Gas Constant
S_i	Carbon selectivity of species i
T	Absolute Temperature
V	Volume of piece of equipment
V_o	Volume of reference piece of equipment
$W_{k,i}$	Unit work required for sub-system k to process species i
X	Production basis for process
Y_i	Yield of species i
Z_i	Name of product species i
v_i	Stoichiometric coefficient of species i
η_E	Conventional resource electricity conversion efficiency
η_H	Natural gas to process heat conversion efficiency
θ	Process scaling factor
γ	Heat capacity ratio
φ	One-pass H_2O conversion

ξ	One-pass CO_2 conversion
Ψ_{CO2}	Ratio of unreacted CO_2 that is recycled
Ψ_{H2O}	Ratio of unreacted H_2O that is recycled

References

1. G. Centi and S. Perathoner, *Catal. Today*, 2009, **148**, 191-205.
2. Nathan S. Lewis, E. Warren, J. McKone, H. B. Gray, P. Agbo, B. D. Stubbert, K. Yokoyama, H. A. Atwater and A. J. Leenheer, *Artificial Photosynthesis: Membrane Supported Assemblies That Use Sunlight to Split Water*, 2011.
3. N. S. Lewis and D. G. Nocera, *Proc. Natl. Acad. Sci.*, 2006, **103**, 15729-15735.
4. G. Centi, E. A. Quadrelli and S. Perathoner, *Energy Environ. Sci.*, 2013, **6**, 1711-1731.
5. D. T. Whipple and P. J. A. Kenis, *J. Phys. Chem. Lett.*, 2010, **1**, 3451-3458.
6. A. Steinfeld, *Sol. Energy*, 2005, **78**, 603-615.
7. B. A. Pinaud, J. D. Benck, L. C. Seitz, A. J. Forman, Z. B. Chen, T. G. Deutsch, B. D. James, K. N. Baum, G. N. Baum, S. Ardo, H. L. Wang, E. Miller and T. F. Jaramillo, *Energy Environ. Sci.*, 2013, **6**, 1983-2002.
8. S. C. Roy, O. K. Varghese, M. Paulose and C. A. Grimes, *ACS Nano*, 2010, **4**, 1259-1278.
9. N. S. Lewis and G. Crabtree, *Basic Research Needs for Solar Energy Utilization*, B. E. Sciences, Department of Energy, 2005.
10. M. G. Walter, E. L. Warren, J. R. McKone, S. W. Boettcher, Q. Mi, E. A. Santori and N. S. Lewis, *Chem. Rev.*, 2010, **110**, 6446-6473.
11. J. Newman, P. G. Hoertz, C. A. Bonino and J. A. Trainham, *J. Electrochem. Soc.*, 2012, **159**, A1722-A1729.
12. O. S. Joo, K. D. Jung, I. Moon, A. Y. Rozovskii, G. I. Lin, S. H. Han and S. J. Uhm, *Ind. Eng. Chem. Res.*, 1999, **38**, 1808-1812.
13. Solar Fuels Institute, http://www.solar-fuels.org/, Accessed June, 2014.
14. Research Triangle Solar Fuels Institute, http://www.solarfuels.org/, Accessed June, 2014.
15. Liquid Light, http://llchemical.com/technology, Accessed June, 2014.
16. ETOGAS: Smart Energy Conversion, http://www.etogas.com/, Accessed June, 2014.
17. SOLAR-JET: Zero-carbon Jet Fuel from Sunlight, http://www.solar-jet.aero/, Accessed June, 2014.
18. Reference Solar Spectral Irradiance: Air Mass 1.5, http://rredc.nrel.gov/solar/spectra/am1.5/, Accessed June, 2014.
19. J. Duffie and W. Beckman, *Solar Engineering of Thermal Processes*, Wiley, Hoboken, NJ, 2006.
20. M. Iqbal, *An Introduction to Solar Radiation*, Academic Press, Toronto, 1983.
21. D. G. Erbs, S. A. Klein and J. A. Duffie, *Sol. Energy*, 1982, **28**, 293-302.
22. Solar Resource Information, http://www.nrel.gov/rredc/solar_resource.html, Accessed June, 2014.
23. World Map of Global Horizontal Irradiation, http://solargis.info/doc/_pics/freemaps/1000px/ghi/SolarGIS-Solar-map-World-map-en.png, Accessed June, 2014.
24. *World Energy Assessment Report: Energy and the Challenge of Sustainability*, U. N. D. Program, United Nations, New York, 2003.
25. Y. Tian and C. Y. Zhao, *Appl. Energy*, 2013, **104**, 538-553.
26. M. A. Alghoul, M. Y. Sulaiman, B. Z. Azmi and M. A. Wahab, *Anti-Corros. Methods Mater.*, 2005, **52**, 199-206.
27. D. F. Ollis, E. Pelizzetti and N. Serpone, *Environ. Sci. Technol.*, 1991, **25**, 1522-1529.
28. M. R. Hoffmann, S. T. Martin, W. Y. Choi and D. W. Bahnemann, *Chem. Rev.*, 1995, **95**, 69-96.
29. R. Reisfeld, *Opt. Mater.*, 2010, **32**, 850-856.
30. *Concentrating Solar Power*, International Renewable Energy Agency, 2012.
31. S. Mekhilef, R. Saidur and A. Safari, *Renewable Sustainable Energy Rev.*, 2011, **15**, 1777-1790.
32. M. Thirugnanasambandam, S. Iniyan and R. Goic, *Renewable Sustainable Energy Rev.*, 2010, **14**, 312-322.

33.   S. Kalogirou, *Appl. Energy*, 2003, **76**, 337-361.
34.   C. Perkins and A. W. Weimer, *AIChE J.*, 2009, **55**, 286-293.
35.   T. Kodama, *Prog. Energy Combust. Sci.*, 2003, **29**, 567-597.
36.   V. Fthenakis, J. E. Mason and K. Zweibel, *Energy Policy*, 2009, **37**, 387-399.
37.   E. Skoplaki and J. A. Palyvos, *Sol. Energy*, 2009, **83**, 614-624.
38.   A. Royne, C. J. Dey and D. R. Mills, *Sol. Energy Mater. Sol. Cells*, 2005, **86**, 451-483.
39.   B. Parida, S. Iniyan and R. Goic, *Renewable Sustainable Energy Rev.*, 2011, **15**, 1625-1636.
40.   L. El Chaar, L. A. lamont and N. El Zein, *Renewable Sustainable Energy Rev.*, 2011, **15**, 2165-2175.
41.   T. M. Razykov, C. S. Ferekides, D. Morel, E. Stefanakos, H. S. Ullal and H. M. Upadhyaya, *Sol. Energy*, 2011, **85**, 1580-1608.
42.   Best Research-Cell Efficiencies, http://www.nrel.gov/ncpv/images/efficiency_chart.jpg, Accessed June, 2014.
43.   M. A. Green, J. Zhao, A. Wang and S. R. Wenham, *Sol. Energy Mater. Sol. Cells*, 2001, **65**, 9-16.
44.   H. Cotal, C. Fetzer, J. Boisvert, G. Kinsey, R. King, P. Hebert, H. Yoon and N. Karam, *Energy Environ. Sci.*, 2009, **2**, 174-192.
45.   S. Gall and B. Rech, *Sol. Energy Mater. Sol. Cells*, 2013, **119**, 306-308.
46.   W. Shockley and H. J. Queisser, *J. Appl. Phys.*, 1961, **32**, 510-519.
47.   Eight Generations of Advancements Lead to Multijunction Solar Cell & Photovoltaic Technology Integration, http://amonix.com/content/eight-generations, Accessed May, 2014.
48.   X. F. Wang, M. R. Khan, M. A. Alam and M. Lundstrom, *2012 38th Ieee Photovoltaic Specialists Conference (Pvsc)*, 2012, 2117-2121.
49.   Sharp Develops Concentrator Solar Cell with World's Highest Conversion Efficiency of 44.4%, http://sharp-world.com/corporate/news/130614.html, Accessed June, 2014.
50.   A. Devos, *J Phys D Appl Phys*, 1980, **13**, 839-846.
51.   M. Grätzel, *Inorg. Chem.*, 2005, **44**, 6841-6851.
52.   M. Grätzel, *J. Photochem. Photobiol., C*, 2003, **4**, 145-153.
53.   H. Hoppe and N. S. Sariciftci, *J. Mater. Res.*, 2004, **19**, 1924-1945.
54.   C. M. Fella, Y. E. Romanyuk and A. N. Tiwari, *Sol. Energy Mater. Sol. Cells*, 2013, **119**, 276-277.
55.   A. J. Nozik, *Nano Lett.*, 2010, **10**, 2735-2741.
56.   *Annual Energy Outlook 2013*, U.S. Energy Information Administration, 2013.
57.   D. Barlev, R. Vidu and P. Stroeve, *Sol. Energy Mater. Sol. Cells*, 2011, **95**, 2703-2725.
58.   H. L. Zhang, J. Baeyens, J. Degreve and G. Caceres, *Renewable Sustainable Energy Rev.*, 2013, **22**, 466-481.
59.   D. Mills, *Sol. Energy*, 2004, **76**, 19-31.
60.   H. L. Zhang, J. Baeyens, J. Degrève and G. Cacères, *Renewable Sustainable Energy Rev.*, 2013, **22**, 466-481.
61.   V. Siva Reddy, S. C. Kaushik, K. R. Ranjan and S. K. Tyagi, *Renewable Sustainable Energy Rev.*, 2013, **27**, 258-273.
62.   A. Gil, M. Medrano, I. Martorell, A. Lazaro, P. Dolado, B. Zalba and L. F. Cabeza, *Renewable Sustainable Energy Rev.*, 2010, **14**, 31-55.
63.   B. Dunn, H. Kamath and J. M. Tarascon, *Science*, 2011, **334**, 928-935.
64.   R. Sioshansi and P. Denholm, *IEEE Trans. Sustainable Energy*, 2010, **1**, 173-183.
65.   J. F. Kenny, N. L. Barber, S. S. Hutson, K. S. Linsey, J. K. Lovelace and M. A. Maupin, *Estimated use of water in the United States in 2005*, U.S. Geological Survey, Reston, VA, 2009.
66.   K. Averyt, J. Fisher, A. Huber-Lee, A. Lewis, J. Macknick, N. Madden, J. Rogers and S. Tellinghuisen, *Freshwater use by U.S. power plants: Electricity's thirst for a precious resource*, Union of Concerned Scientists, Cambridge, MA, 2011.
67.   *Energy demands on water resources*, U. S. Department of Energy, 2006.

68.   L. Espinal, D. L. Poster, W. Wong-Ng, A. J. Allen and M. L. Green, *Environ. Sci. Technol.*, 2013, **47**, 11960-11975.

69.   *Inventory of U.S. Greenhouse Gas Emissions and Sinks 1990-2011.*, U.S. Environmental Protection Agency, 2013.

70.   B. P. Spigarelli and S. K. Kawatra, *J. CO2 Util.*, 2013, **1**, 69-87.

71.   K. Damen, M. van Troost, A. Faaij and W. Turkenburg, *Prog. Energy Combust. Sci.*, 2006, **32**, 215-246.

72.   M. Kanniche, R. Gros-Bonnivard, P. Jaud, J. Valle-Marcos, J. M. Amann and C. Bouallou, *Appl. Therm. Eng.*, 2010, **30**, 53-62.

73.   T. F. Wall, *Proceedings of the Combustion Institute*, 2007, **31**, 31-47.

74.   H. W. Pennline, D. R. Luebke, K. L. Jones, C. R. Myers, B. I. Morsi, Y. J. Heintz and J. B. Ilconich, *Fuel Process. Technol.*, 2008, **89**, 897-907.

75.   D. Berstad, R. Anantharaman and P. Neksa, *International Journal of Refrigeration-Revue Internationale Du Froid*, 2013, **36**, 1403-1416.

76.   J. Adanez, A. Abad, F. Garcia-Labiano, P. Gayan and L. F. de Diego, *Prog. Energy Combust. Sci.*, 2012, **38**, 215-282.

77.   P. Noothout, F. Wiersma, O. Hurtado, P. Roelofsen and D. Macdonald, *CO_2 Pipeline Infrastructure*, International Energy Agency, 2013.

78.   T. Grant, D. Morgan and K. Gerdes, *Carbon dioxide transport and storage costs in NETL studies*, N. E. T. Laboratory, U.S. Department of Energy, 2013.

79.   D. Aaron and C. Tsouris, *Sep. Sci. Technol.*, 2005, **40**, 321-348.

80.   S. Choi, J. H. Drese and C. W. Jones, *Chemsuschem*, 2009, **2**, 796-854.

81.   D. M. D'Alessandro, B. Smit and J. R. Long, *Angew. Chem. Int. Ed.*, 2010, **49**, 6058-6082.

82.   C. W. Jones, *Annual Review of Chemical and Biomolecular Engineering, Vol 2*, 2011, **2**, 31-52.

83.   M. K. Mondal, H. K. Balsora and P. Varshney, *Energy*, 2012, **46**, 431-441.

84.   N. MacDowell, N. Florin, A. Buchard, J. Hallett, A. Galindo, G. Jackson, C. S. Adjiman, C. K. Williams, N. Shah and P. Fennell, *Energy Environ. Sci.*, 2010, **3**, 1645-1669.

85.   P. Folger, E. S. Rubin, A. Marks, H. Mantripragada, P. Versteed and J. Kitchin, *Carbon capture: a technology assessment*, Carnegie Mellon University, 2013.

86.   O. Aschenbrenner and P. Styring, *Energy Environ. Sci.*, 2010, **3**, 1106-1113.

87.   G. T. Rochelle, *Science*, 2009, **325**, 1652-1654.

88.   A. Dibenedetto, M. Aresta, C. Fragale and M. Narracci, *Green Chem.*, 2002, **4**, 439-443.

89.   J. T. Yeh and H. W. Pennline, *Energy Fuels*, 2001, **15**, 274-278.

90.   P. D. Vaidya and E. Y. Kenig, *Chem. Eng. Technol.*, 2007, **30**, 1467-1474.

91.   W. Conway, X. G. Wang, D. Fernandes, R. Burns, G. Lawrance, G. Puxty and M. Maeder, *Environ. Sci. Technol.*, 2013, **47**, 1163-1169.

92.   J. E. Bara, T. K. Carlisle, C. J. Gabriel, D. Camper, A. Finotello, D. L. Gin and R. D. Noble, *Ind. Eng. Chem. Res.*, 2009, **48**, 2739-2751.

93.   J. E. Bara, D. E. Camper, D. L. Gin and R. D. Noble, *Acc. Chem. Res.*, 2010, **43**, 152-159.

94.   D. Wappel, G. Gronald, R. Kalb and J. Draxler, *Int. J. Greenh. Gas Control*, 2010, **4**, 486-494.

95.   M. Hasib-ur-Rahman, M. Siaj and F. Larachi, *Chem. Eng. Process.*, 2010, **49**, 313-322.

96.   Z. Yong, V. Mata and A. E. Rodrigues, *Sep. Purif. Technol.*, 2002, **26**, 195-205.

97.   R. V. Siriwardane, M. S. Shen, E. P. Fisher and J. A. Poston, *Energy Fuels*, 2001, **15**, 279-284.

98.   S. Keskin, T. M. van Heest and D. S. Sholl, *Chemsuschem*, 2010, **3**, 879-891.

99.   J. R. Li, R. J. Kuppler and H. C. Zhou, *Chem. Soc. Rev.*, 2009, **38**, 1477-1504.

100.   A. Phan, C. J. Doonan, F. J. Uribe-Romo, C. B. Knobler, M. O'Keeffe and O. M. Yaghi, *Acc. Chem. Res.*, 2010, **43**, 58-67.

101.   J. C. Hicks, J. H. Drese, D. J. Fauth, M. L. Gray, G. G. Qi and C. W. Jones, *J. Am. Chem. Soc.*, 2008, **130**, 2902-2903.
102.   X. C. Xu, C. S. Song, J. M. Andresen, B. G. Miller and A. W. Scaroni, *Energy Fuels*, 2002, **16**, 1463-1469.
103.   Y. Belmabkhout and A. Sayari, *Adsorption*, 2009, **15**, 318-328.
104.   P. J. E. Harlick and A. Sayari, *Ind. Eng. Chem. Res.*, 2007, **46**, 446-458.
105.   T. Tsuda and T. Fujiwara, *J. Chem. Soc. Chem. Comm.*, 1992, 1659-1661.
106.   J. H. Drese, S. Choi, R. P. Lively, W. J. Koros, D. J. Fauth, M. L. Gray and C. W. Jones, *Adv. Funct. Mater.*, 2009, **19**, 3821-3832.
107.   E. J. Anthony, *Ind. Eng. Chem. Res.*, 2008, **47**, 1747-1754.
108.   G. Grasa, B. GonzAlez, M. Alonso and J. C. Abanades, *Energy Fuels*, 2007, **21**, 3560-3562.
109.   A. Hanif, S. Dasgupta, S. Divekar, A. Arya, M. O. Garg and A. Nanoti, *Chem. Eng. J.*, 2014, **236**, 91-99.
110.   A. D. Ebner and J. A. Ritter, *Sep. Sci. Technol.*, 2009, **44**, 1273-1421.
111.   C. E. Powell and G. G. Qiao, *J. Membrane Sci.*, 2006, **279**, 1-49.
112.   J. Zou and W. S. W. Ho, *J. Membrane Sci.*, 2006, **286**, 310-321.
113.   P. Scovazzo, J. Kieft, D. A. Finan, C. Koval, D. DuBois and R. Noble, *J. Membrane Sci.*, 2004, **238**, 57-63.
114.   T. S. Chung, L. Y. Jiang, Y. Li and S. Kulprathipanja, *Prog. Polym. Sci.*, 2007, **32**, 483-507.
115.   X. Q. Pan, D. Clodic and J. Toubassy, *Greenhouse Gases-Science and Technology*, 2013, **3**, 8-20.
116.   D. Clodic and M. Younes, A new method for CO2 capture: Frosting CO2 at atmospheric pressure, Kyoto, Japan, 2002.
117.   eGRID, http://www.epa.gov/cleanenergy/energy-resources/egrid/, Accessed May, 2014.
118.   M. J. Tuinier, H. P. Hamers and M. V. Annaland, *Int. J. Greenh. Gas Control*, 2011, **5**, 1559-1565.
119.   J. van Straelen, F. Geuzebroek, N. Goodchild, G. Protopapas and L. Mahony, *Int. J. Greenh. Gas Control*, 2010, **4**, 316-320.
120.   M. R. M. Abu-Zahra, J. P. M. Niederer, P. H. M. Feron and G. F. Versteeg, *Int. J. Greenh. Gas Control*, 2007, **1**, 135-142.
121.   *Carbon Capture & Storage: Assessing the Economics*, M. C. C. Initiative, McKinsey & Company, 2008.
122.   T. C. Merkel, H. Q. Lin, X. T. Wei and R. Baker, *J. Membrane Sci.*, 2010, **359**, 126-139.
123.   J. D. Holladay, J. Hu, D. L. King and Y. Wang, *Catal. Today*, 2009, **139**, 244-260.
124.   T. Ramsden, D. Steward and J. Zuboy, *Analyzing the levelized cost of centralized and distributed hydrogen production using the H2A production model, version 2*, N. R. E. Laboratory, U.S. Department of Energy, 2009.
125.   Q. A. Wang, J. Z. Luo, Z. Y. Zhong and A. Borgna, *Energy Environ. Sci.*, 2011, **4**, 42-55.
126.   A. Ursua, L. M. Gandia and P. Sanchis, *P. IEEE*, 2012, **100**, 410-426.
127.   C. A. Grimes, O. K. Varghese and S. Ranjan, *Light, Water, Hydrogen: The Solar generation of Hydrogen by Water Photoelectrolysis*, Springer US, 2008.
128.   J. Ivy, *Summary of Electrolytic Hydrogen Production*, N. R. E. Laboratory, U.S. Department of Energy, 2004.
129.   T. L. Gibson and N. A. Kelly, *Int. J. Hydrogen Energy*, 2008, **33**, 5931-5940.
130.   J. E. Genovese, K. Harg, M. Paster and J. A. Turner, *Current (2009) state-of-the-art hydrogen production cost estimate using water electrolysis*, N. R. E. Laboratory, U.S. Department of Energy, 2009.
131.   K. Zeng and D. K. Zhang, *Prog. Energy Combust. Sci.*, 2010, **36**, 307-326.
132.   M. J. Giz, J. C. P. Silva, M. Ferreira, S. A. S. Machado, E. A. Ticianelli, L. A. Avaca and E. R. Gonzalez, *Int. J. Hydrogen Energy*, 1992, **17**, 725-729.

133.   F. C. Crnkovic, S. A. S. Machado and L. A. Avaca, *Int. J. Hydrogen Energy*, 2004, **29**, 249-254.
134.   I. A. Raj, *J. Mater. Sci.*, 1993, **28**, 4375-4382.
135.   M. S. El-Deab, M. I. Awad, A. M. Mohammad and T. Ohsaka, *Electrochem. Commun.*, 2007, **9**, 2082-2087.
136.   R. N. Singh, D. Mishra, Anindita, A. S. K. Sinha and A. Singh, *Electrochem. Commun.*, 2007, **9**, 1369-1373.
137.   H. Wendt, H. Hofmann and V. Plzak, *Mater. Chem. Phys.*, 1989, **22**, 27-49.
138.   M. Carmo, D. L. Fritz, J. Merge and D. Stolten, *Int. J. Hydrogen Energy*, 2013, **38**, 4901-4934.
139.   S. A. Grigoriev, V. I. Porembsky and V. N. Fateev, *Int. J. Hydrogen Energy*, 2006, **31**, 171-175.
140.   P. Millet, N. Mbemba, S. A. Grigoriev, V. N. Fateev, A. Aukauloo and C. Etievant, *Int. J. Hydrogen Energy*, 2011, **36**, 4134-4142.
141.   F. Barbir, *Sol. Energy*, 2005, **78**, 661-669.
142.   A. Goni-Urtiaga, D. Presvytes and K. Scott, *Int. J. Hydrogen Energy*, 2012, **37**, 3358-3372.
143.   H. Ito, T. Maeda, A. Nakano and H. Takenaka, *Int. J. Hydrogen Energy*, 2011, **36**, 10527-10540.
144.   W. F. Chen, J. T. Muckerman and E. Fujita, *Chem. Commun.*, 2013, **49**, 8896-8909.
145.   D. V. Esposito, S. T. Hunt, A. L. Stottlemyer, K. D. Dobson, B. E. McCandless, R. W. Birkmire and J. G. G. Chen, *Angew. Chem. Int. Ed.*, 2010, **49**, 9859-9862.
146.   C. Felix, T. Maiyalagan, S. Pasupathi, B. Bladergroen and V. Linkov, *Int. J. Electrochem. Sci.*, 2012, **7**, 12064-12077.
147.   E. Mayousse, F. Maillard, F. Fouda-Onana, O. Sicardy and N. Guillet, *Int. J. Hydrogen Energy*, 2011, **36**, 10474-10481.
148.   C. B. Xu, L. R. Ma, J. L. Li, W. Zhao and Z. X. Gan, *Int. J. Hydrogen Energy*, 2012, **37**, 2985-2992.
149.   A. Marshall, B. Borresen, G. Hagen, M. Tsypkin and R. Tunold, *Electrochim. Acta*, 2006, **51**, 3161-3167.
150.   J. M. Spurgeon and N. S. Lewis, *Energy Environ. Sci.*, 2011, **4**, 2993-2998.
151.   K. D. Kreuer, *Solid State Ionics*, 1997, **97**, 1-15.
152.   C. A. Linkous, H. R. Anderson, R. W. Kopitzke and G. L. Nelson, *Int. J. Hydrogen Energy*, 1998, **23**, 525-529.
153.   R. J. Gorte and J. M. Vohs, *Annual Review of Chemical and Biomolecular Engineering, Vol 2*, 2011, **2**, 9-30.
154.   M. A. Laguna-Bercero, *J. Power Sources*, 2012, **203**, 4-16.
155.   M. Ni, M. K. H. Leung and D. Y. C. Leung, *Int. J. Hydrogen Energy*, 2008, **33**, 2337-2354.
156.   H. S. Hong, U. S. Chae, S. T. Choo and K. S. Lee, *J. Power Sources*, 2005, **149**, 84-89.
157.   M. D. Liang, B. Yu, M. F. Wen, J. Chen, J. M. Xu and Y. C. Zhai, *J. Power Sources*, 2009, **190**, 341-345.
158.   C. H. Yang, A. Coffin and F. L. Chen, *Int. J. Hydrogen Energy*, 2010, **35**, 3221-3226.
159.   *The Hydrogen Economy: Opportunities, Costs, Barriers, and R&D Needs*, Natrional Research Council and National Academy of Engineering, Washington D.C., 2004.
160.   T. Bak, J. Nowotny, M. Rekas and C. C. Sorrell, *Int. J. Hydrogen Energy*, 2002, **27**, 991-1022.
161.   A. Fujishima and K. Honda, *Nature*, 1972, **238**, 37-+.
162.   A. J. Nozik, *Annu. Rev. Phys. Chem.*, 1978, **29**, 189-222.
163.   D. A. Tryk, A. Fujishima and K. Honda, *Electrochim. Acta*, 2000, **45**, 2363-2376.
164.   M. Gratzel, *Nature*, 2001, **414**, 338-344.
165.   R. Abe, *J. Photochem. Photobiol. C Rev.*, 2010, **11**, 179-209.
166.   A. B. Murphy, P. R. F. Barnes, L. K. Randeniya, I. C. Plumb, I. E. Grey, M. D. Horne and J. A. Glasscock, *Int. J. Hydrogen Energy*, 2006, **31**, 1999-2017.
167.   A. K. Ghosh and H. P. Maruska, *J. Electrochem. Soc.*, 1977, **124**, 1516-1522.

168. J. F. Houlihan, D. B. Armitage, T. Hoovler, D. Bonaquist, D. P. Madacsi and L. N. Mulay, *Mater. Res. Bull.*, 1978, **13**, 1205-1212.
169. C. Santato, M. Ulmann and J. Augustynski, *J. Phys. Chem. B*, 2001, **105**, 936-940.
170. H. L. Wang, T. Lindgren, J. J. He, A. Hagfeldt and S. E. Lindquist, *J. Phys. Chem. B*, 2000, **104**, 5686-5696.
171. A. Iwase and A. Kudo, *J. Mater. Chem.*, 2010, **20**, 7536-7542.
172. K. Sayama, A. Nomura, Z. G. Zou, R. Abe, Y. Abe and H. Arakawa, *Chem. Commun.*, 2003, 2908-2909.
173. J. Z. Su, L. J. Guo, S. Yoriya and C. A. Grimes, *Crystal Growth & Design*, 2010, **10**, 856-861.
174. A. Duret and M. Gratzel, *J. Phys. Chem. B*, 2005, **109**, 17184-17191.
175. J. H. Kennedy and K. W. Frese, *J. Electrochem. Soc.*, 1977, **124**, C130-C130.
176. C. Sanchez, M. Hendewerk, K. D. Sieber and G. A. Somorjai, *J. Solid State Chem.*, 1986, **61**, 47-55.
177. R. Abe, T. Takata, H. Sugihara and K. Domen, *Chem. Lett.*, 2005, **34**, 1162-1163.
178. R. Nakamura, T. Tanaka and Y. Nakato, *J. Phys. Chem. B*, 2005, **109**, 8920-8927.
179. N. Nishimura, B. Raphael, K. Maeda, L. Le Gendre, R. Abe, J. Kubota and K. Domen, *Thin Solid Films*, 2010, **518**, 5855-5859.
180. O. Khaselev and J. A. Turner, *Science*, 1998, **280**, 425-427.
181. S. Licht, B. Wang, S. Mukerji, T. Soga, M. Umeno and H. Tributsch, *J. Phys. Chem. B*, 2000, **104**, 8920-8924.
182. J. N. Nian, C. C. Hu and H. Teng, *Int. J. Hydrogen Energy*, 2008, **33**, 2897-2903.
183. R. van de Krol and M. Gratzel, *Photoelectrochemical Hydrogen Production*, Springer, New York, 2012.
184. S. Y. Reece, J. A. Hamel, K. Sung, T. D. Jarvi, A. J. Esswein, J. J. H. Pijpers and D. G. Nocera, *Science*, 2011, **334**, 645-648.
185. D. A. Lutterman, Y. Surendranath and D. G. Nocera, *J. Am. Chem. Soc.*, 2009, **131**, 3838-+.
186. M. W. Kanan and D. G. Nocera, *Science*, 2008, **321**, 1072-1075.
187. R. van Noorden, *Nature*, 2012.
188. A. Kudo and Y. Miseki, *Chem. Soc. Rev.*, 2009, **38**, 253-278.
189. X. B. Chen, S. H. Shen, L. J. Guo and S. S. Mao, *Chem. Rev.*, 2010, **110**, 6503-6570.
190. A. Kudo, *Int. J. Hydrogen Energy*, 2006, **31**, 197-202.
191. K. Maeda and K. Domen, *J. Phys. Chem.C*, 2007, **111**, 7851-7861.
192. K. Maeda, K. Teramura, D. L. Lu, T. Takata, N. Saito, Y. Inoue and K. Domen, *Nature*, 2006, **440**, 295-295.
193. J. Kubota and K. Domen, *Electrochem. Soc. Interface*, 2013, **22**, 57-62.
194. R. Abe, K. Sayama and H. Sugihara, *J. Phys. Chem. B*, 2005, **109**, 16052-16061.
195. K. Maeda, M. Higashi, D. L. Lu, R. Abe and K. Domen, *J. Am. Chem. Soc.*, 2010, **132**, 5858-5868.
196. Y. Sasaki, A. Iwase, H. Kato and A. Kudo, *J. Catal.*, 2008, **259**, 133-137.
197. S. Linic, P. Christopher and D. B. Ingram, *Nat. Mater.*, 2011, **10**, 911-921.
198. W. R. Pyle, M. H. Hayes and A. L. Spivak, Direct solar-thermal hydrogen production from water using nozzle/skimmer and glow discharge, 1996.
199. C. Perkins and A. W. Weimer, *Int. J. Hydrogen Energy*, 2004, **29**, 1587-1599.
200. C. C. Agrafiotis, C. Pagkoura, S. Lorentzou, M. Kostoglott and A. G. Konstandopoulos, *Catal. Today*, 2007, **127**, 265-277.
201. T. Kodama and N. Gokon, *Chem. Rev.*, 2007, **107**, 4048-4077.
202. R. Perret, *Solar Thermochemical Hydrogen Production Research (STCH): Thermochemical Cycle Selection and Investment Priority*, F. C. T. P. Office of Energy Efficiency & Renewable Energy, U.S. Department of Energy, Livermore, 2011.
203. A. Steinfeld, *Int. J. Hydrogen Energy*, 2002, **27**, 611-619.

204.   P. Charvin, S. Abanades, G. Flamant and F. Lemort, *Energy*, 2007, **32**, 1124-1133.
205.   A. Steinfeld, S. Sanders and R. Palumbo, *Sol. Energy*, 1999, **65**, 43-53.
206.   C. L. Muhich, B. W. Evanko, K. C. Weston, P. Lichty, X. H. Liang, J. Martinek, C. B. Musgrave and A. W. Weimer, *Science*, 2013, **341**, 540-542.
207.   S. Abanades and G. Flamant, *Sol. Energy*, 2006, **80**, 1611-1623.
208.   Y. Tamaura, A. Steinfeld, P. Kuhn and K. Ehrensberger, *Energy*, 1995, **20**, 325-330.
209.   T. Kodama, Y. Kondoh, R. Yamamoto, H. Andou and N. Satou, *Sol. Energy*, 2005, **78**, 623-631.
210.   A. W. Weimer, C. Perkins, P. Lichty, H. Funke, J. Zartman, D. Hirsch, C. Bingham, A. Lewandowski, S. Haussener and A. Steinfeld, *Development of a solar-thermal ZnO/Zn water-splitting thermochemical cycle*, N. R. E. Laboratory, U.S. Department of Energy, 2009.
211.   R. B. Diver, J. E. Miller, M. D. Allendorf, N. P. Siegel and R. E. Hogan, *J. Sol. Energ-T ASME*, 2008, **130**.
212.   J. Kim, C. A. Henao, T. A. Johnson, D. E. Dedrick, J. E. Miller, E. B. Stechel and C. T. Maravelias, *Energy Environ. Sci.*, 2011, **4**, 3122-3132.
213.   J. E. Miller, M. D. Allendorf, R. B. Diver, L. R. Evans, N. P. Siegel and J. N. Stuecker, *J. Mater. Sci.*, 2008, **43**, 4714-4728.
214.   S. Kasahara, S. Kubo, R. Hino, K. Onuki, M. Nomura and S. Nakao, *Int. J. Hydrogen Energy*, 2007, **32**, 489-496.
215.   K. Onuki, S. Kubo, A. Terada, N. Sakaba and R. Hino, *Energy Environ. Sci.*, 2009, **2**, 491-497.
216.   B. J. Xu, Y. Bhawe and M. E. Davis, *Proc. Natl. Acad. Sci. USA*, 2012, **109**, 9260-9264.
217.   Y. Hori, in *Handbook of Fuel Cells - Fundamentals, technology, and applications*, eds. W. Vielstich, H. A. Gasteiger, A. Lamm and H. Yokokawa, John Wiley & Sons, Ltd., 2005.
218.   Y. Hori, *Modern Aspects of Electrochemistry, No 42*, 2008, 89-189.
219.   N. S. Spinner, J. A. Vega and W. E. Mustain, *Catal. Sci. Tech.*, 2012, **2**, 19-28.
220.   *Basic Research Needs: Catalysis for Energy*, B. E. Sciences, U.S. Department of Energy, 2007.
221.   J. L. Qiao, Y. Y. Liu, F. Hong and J. J. Zhang, *Chem. Soc. Rev.*, 2014, **43**, 631-675.
222.   E. E. Benson, C. P. Kubiak, A. J. Sathrum and J. M. Smieja, *Chem. Soc. Rev.*, 2009, **38**, 89-99.
223.   A. Bandi, *J. Electrochem. Soc.*, 1990, **137**, 2157-2160.
224.   J. Yano and S. Yamasaki, *J. Appl. Electrochem.*, 2008, **38**, 1721-1726.
225.   K. Ogura, *J. CO2 Util.*, 2013, **1**, 43-49.
226.   J. P. Qu, X. G. Zhang, Y. G. Wang and C. X. Xie, *Electrochim. Acta*, 2005, **50**, 3576-3580.
227.   K. W. Frese, *J. Electrochem. Soc.*, 1991, **138**, 3338-3344.
228.   M. Le, M. Ren, Z. Zhang, P. T. Sprunger, R. L. Kurtz and J. C. Flake, *J. Electrochem. Soc.*, 2011, **158**, E45-E49.
229.   F. Bidrawn, G. Kim, G. Corre, J. T. S. Irvine, J. M. Vohs and R. J. Gorte, *Electrochem. Solid-State Lett.*, 2008, **11**, B167-B170.
230.   J. Weissbart and W. H. Smart, *Study of electrolytic dissociation of CO2–H2O using a solid oxide electrolyte*, National Aeronautics and Space Administration, 1967.
231.   K. R. Sridhar and B. T. Vaniman, *Solid State Ionics*, 1997, **93**, 321-328.
232.   K. Morikawa, T. Shirasaki and M. Okada, *Adv. Catal.*, 1969, **20**, 97-133.
233.   S. S. Xu, S. S. Li, W. T. Yao, D. H. Dong and K. Xie, *J. Power Sources*, 2013, **230**, 115-121.
234.   C. Graves, S. D. Ebbesen and M. Mogensen, *Solid State Ionics*, 2011, **192**, 398-403.
235.   S. D. Ebbesen, R. Knibbe and M. Mogensen, *J. Electrochem. Soc.*, 2012, **159**, F482-F489.
236.   C. Stoots, J. O'Brien and J. Hartvigsen, *Int. J. Hydrogen Energy*, 2009, **34**, 4208-4215.
237.   Z. Zhan, W. Kobsiriphat, J. R. Wilson, M. Pillai, I. Kim and S. A. Barnett, *Energy Fuels*, 2009, **23**, 3089-3096.
238.   C. Graves, S. D. Ebbesen, M. Mogensen and K. S. Lackner, *Renewable Sustainable Energy Rev.*, 2011, **15**, 1-23.

239. E. J. Dufek, T. E. Lister, S. G. Stone and M. E. McIlwain, *J. Electrochem. Soc.*, 2012, **159**, F514-F517.
240. H. Li and C. Oloman, *J. Appl. Electrochem.*, 2005, **35**, 955-965.
241. D. T. Whipple, E. C. Finke and P. J. A. Kenis, *Electrochem. Solid-State Lett.*, 2010, **13**, D109-D111.
242. K. Xie, Y. Q. Zhang, G. Y. Meng and J. T. S. Irvine, *J. Mater. Chem.*, 2011, **21**, 195-198.
243. B. X. Hu, V. Stancovski, M. Morton and S. L. Suib, *Appl. Catal., A*, 2010, **382**, 277-283.
244. *US Pat.,* 8641885, 2014.
245. *US Pat.,* 8592633, 2013.
246. B. H. Mahan, *J. Chem. Phys.*, 1960, **33**, 959.
247. A. Corma and H. Garcia, *J. Catal.*, 2013, **308**, 168-175.
248. F. Sastre, A. Corma and H. Garcia, *J. Am. Chem. Soc.*, 2012, **134**, 14137-14141.
249. B. Kumar, M. Llorente, J. Froehlich, T. Dang, A. Sathrum and C. P. Kubiak, *Annual Review of Physical Chemistry, Vol 63*, 2012, **63**, 541-+.
250. R. Hinogami, Y. Nakamura, S. Yae and Y. Nakato, *J. Phys. Chem. B*, 1998, **102**, 974-980.
251. K. Hara, A. Kudo and T. Sakata, *J. Electroanal. Chem.*, 1995, **391**, 141-147.
252. I. Taniguchi, B. Aurianblajeni and J. O. M. Bockris, *Electrochim. Acta*, 1984, **29**, 923-932.
253. H. Yoneyama, K. Sugimura and S. Kuwabata, *J. Electroanal. Chem.*, 1988, **249**, 143-153.
254. Y. Taniguchi, H. Yoneyama and H. Tamura, *Bull. Chem. Soc. Jpn.*, 1982, **55**, 2034-2039.
255. S. Ikeda, Y. Saito, M. Yoshida, H. Noda, M. Maeda and K. Ito, *J. Electroanal. Chem.*, 1989, **260**, 335-345.
256. W. M. Sears and S. R. Morrison, *J. Phys. Chem.*, 1985, **89**, 3295-3298.
257. K. W. Frese and D. Canfield, *J. Electrochem. Soc.*, 1984, **131**, 2518-2522.
258. Y. Nakamura, R. Hinogami, S. Yae and Y. Nakato, *Advances in Chemical Conversions for Mitigating Carbon Dioxide*, 1998, **114**, 565-568.
259. S. Kaneco, H. Katsumata, T. Suzuki and K. Ohta, *Appl. Catal., B*, 2006, **64**, 139-145.
260. H. Flaisher, R. Tenne and M. Halmann, *J. Electroanal. Chem.*, 1996, **402**, 97-105.
261. B. Aurianblajeni, I. Taniguchi and J. O. Bockris, *J. Electroanal. Chem.*, 1983, **149**, 291-293.
262. C. R. Cabrera and H. D. Abruna, *J. Electroanal. Chem.*, 1986, **209**, 101-107.
263. T. Inoue, A. Fujishima, S. Konishi and K. Honda, *Nature*, 1979, **277**, 637-638.
264. P. Usubharatana, D. McMartin, A. Veawab and P. Tontiwachwuthikul, *Ind. Eng. Chem. Res.*, 2006, **45**, 2558-2568.
265. S. Y. Qin, F. Xin, Y. D. Liu, X. H. Yin and W. Ma, *J. Colloid Interface Sci.*, 2011, **356**, 257-261.
266. Q. H. Zhang, W. D. Han, Y. J. Hong and J. G. Yu, *Catal. Today*, 2009, **148**, 335-340.
267. K. Koci, K. Mateju, L. Obalova, S. Krejcikova, Z. Lacny, D. Placha, L. Capek, A. Hospodkova and O. Solcova, *Appl. Catal., B*, 2010, **96**, 239-244.
268. Y. Li, W. N. Wang, Z. L. Zhan, M. H. Woo, C. Y. Wu and P. Biswas, *Appl. Catal., B*, 2010, **100**, 386-392.
269. K. Koci, L. Obalova, L. Matejova, D. Placha, Z. Lacny, J. Jirkovsky and O. Solcova, *Appl. Catal., B*, 2009, **89**, 494-502.
270. M. Anpo, H. Yamashita, Y. Ichihashi and S. Ehara, *J. Electroanal. Chem.*, 1995, **396**, 21-26.
271. K. Mori, H. Yamashita and M. Anpo, *R. Soc. Chem. Adv.*, 2012, **2**, 3165-3172.
272. M. Kitano, M. Matsuoka, M. Ueshima and M. Anpo, *Appl. Catal., A*, 2007, **325**, 1-14.
273. M. Iwasaki, M. Hara, H. Kawada, H. Tada and S. Ito, *J. Colloid Interface Sci.*, 2000, **224**, 202-204.
274. M. Tahir and N. S. Amin, *Appl. Catal., A*, 2013, **467**, 483-496.
275. T. V. Nguyen and J. C. S. Wu, *Sol. Energy Mater. Sol. Cells*, 2008, **92**, 864-872.
276. Q. Y. Zhang, Y. Li, E. A. Ackerman, M. Gajdardziska-Josifovska and H. L. Li, *Appl. Catal., A*, 2011, **400**, 195-202.
277. Z. H. Zhao, J. M. Fan, J. Y. Wang and R. F. Li, *Catal. Commun.*, 2012, **21**, 32-37.

278.   W. B. Hou, W. H. Hung, P. Pavaskar, A. Goeppert, M. Aykol and S. B. Cronin, *ACS Catal.*, 2011, **1**, 929-936.

279.   O. Ishitani, C. Inoue, Y. Suzuki and T. Ibusuki, *J. Photoch. Photobio. A*, 1993, **72**, 269-271.

280.   K. Tennakone, *Sol. Energ. Mater.*, 1984, **10**, 235-238.

281.   M. L. Perry, J. Newman and E. J. Cairns, *J. Electrochem. Soc.*, 1998, **145**, 5-15.

282.   N. Furuya, T. Yamazaki and M. Shibata, *J. Electroanal. Chem.*, 1997, **431**, 39-41.

283.   K. Hara and T. Sakata, *J. Electrochem. Soc.*, 1997, **144**, 539-545.

284.   Y. Tomita, S. Teruya, O. Koga and Y. Hori, *J. Electrochem. Soc.*, 2000, **147**, 4164-4167.

285.   S. Kaneco, K. Iiba, N. Hiei, K. Ohta, T. Mizuno and T. Suzuki, *Electrochim. Acta*, 1999, **44**, 4701-4706.

286.   K. Ogura and N. Endo, *J. Electrochem. Soc.*, 1999, **146**, 3736-3740.

287.   D. R. MacFarlane, N. Tachikawa, M. Forsyth, J. M. Pringle, P. C. Howlett, G. D. Elliott, J. H. Davis, M. Watanabe, P. Simon and C. A. Angell, *Energy Environ. Sci.*, 2014, **7**, 232-250.

288.   M. V. Fedorov and A. A. Kornyshev, *Chem. Rev.*, 2014, **114**, 2978-3036.

289.   P. Hapiot and C. Lagrost, *Chem. Rev.*, 2008, **108**, 2238-2264.

290.   L. R. Martin, *Sol. Energy*, 1980, **24**, 271-277.

291.   M. E. Galvez, P. G. Loutzenhiser, I. Hischier and A. Steinfeld, *Energy Fuels*, 2008, **22**, 3544-3550.

292.   A. J. Traynor and R. J. Jensen, *Ind. Eng. Chem. Res.*, 2002, **41**, 1935-1939.

293.   D. Arifin, V. J. Aston, X. H. Liang, A. H. McDaniel and A. W. Weimer, *Energy Environ. Sci.*, 2012, **5**, 9438-9443.

294.   S. Abanades and M. Chambon, *Energy Fuels*, 2010, **24**, 6667-6674.

295.   N. Gokon, H. Murayama, A. Nagasaki and T. Kodama, *Sol. Energy*, 2009, **83**, 527-537.

296.   T. Kodama, N. Gokon and R. Yamamoto, *Sol. Energy*, 2008, **82**, 73-79.

297.   M. D. Allendorf, R. B. Diver, N. P. Siegel and J. E. Miller, *Energy Fuels*, 2008, **22**, 4115-4124.

298.   J. R. Scheffe, J. H. Li and A. W. Weimer, *Int. J. Hydrogen Energy*, 2010, **35**, 3333-3340.

299.   W. C. Chueh and S. M. Haile, *Philos. T. Roy. Soc. A*, 2010, **368**, 3269-3294.

300.   W. C. Chueh, C. Falter, M. Abbott, D. Scipio, P. Furler, S. M. Haile and A. Steinfeld, *Science*, 2010, **330**, 1797-1801.

301.   J. Kim, T. A. Johnson, J. E. Miller, E. B. Stechel and C. T. Maravelias, *Energy Environ. Sci.*, 2012, **5**, 8417-8429.

302.   *Annual Energy Review 2011*, U.S. Energy Information Administration, 2011.

303.   *Solar Photovoltaic Cell/Module Shipments Report 2012*, U.S. Energy Information Administration, 2013.

304.   K. Ikeue, S. Nozaki, M. Ogawa and M. Anpo, *Catal. Lett.*, 2002, **80**, 111-114.

305.   *UOP Selexol Technology for Acid Gas Removal*, UOP LLC, 2009.

306.   B. Burr and L. Lyddon, *A Comparison of Physical Solvents for Acid Gas Removal*, Bryan Research & Engineering, Inc.

307.   C. Chen, Ph.D., Carnegie Mellon, 2005.

308.   *Electric Sales, Revenue, and average price*, U.S. Energy Information Administration, 2013.

309.   R. Silva, M. Berenguel, M. Perez and A. Fernandez-Garcia, *Appl. Energy*, 2014, **113**, 603-614.

310.   J. C. S. Wu, T. H. Wu, T. C. Chu, H. J. Huang and D. P. Tsai, *Top. Catal.*, 2008, **47**, 131-136.

311.   E. V. Kondratenko, G. Mul, J. Baltrusaitis, G. O. Larrazabal and J. Perez-Ramirez, *Energy Environ. Sci.*, 2013, **6**, 3112-3135.

312.   C. H. Bartholomew and R. J. Farrauto, *Fundamentals of Industrial Catalytic Processes*, Wiley-AIChE, Hoboken, NJ, 2005.